A posteriori error analysis of a mixed virtual element method for a nonlinear Brinkman model of porous media flow

Mauricio Munar, Filander A. Sequeira

PREPRINT 2019-45

SERIE DE PRE-PUBLICACIONES

A posteriori error analysis of a mixed virtual element method for a nonlinear Brinkman model of porous media flow

Mauricio Munar* Filánder A. Sequeira†

Abstract

In this paper we present an a posteriori error analysis of a mixed-VEM discretization for a nonlinear Brinkman model of porous media flow, which has been proposed by the authors in a previous work. Therein, the system is formulated in terms of a pseudostress tensor and the velocity gradient, whereas the velocity and the pressure of the fluid are computed via postprocessing formulae. Furthermore, the well-posedness of the associated augmented formulation along with a priori error bounds for the discrete scheme also were established. We now propose reliable and efficient residual-based a posteriori error estimates for a computable approximation of the virtual solution associated to the aforementioned problem. The resulting error estimator is fully computable from the degrees of freedom of the solutions and applies on very general polygonal meshes. For the analysis we make use of a global inf-sup condition, Helmholtz decomposition, local approximation properties of interpolation operators and inverse inequalities together with localization arguments based on bubble functions. Finally, we provide some numerical results confirming the properties of our estimator and illustrating the good performance of the associated adaptive algorithm.

Key words: mixed virtual element method, nonlinear Brinkman model, a posteriori error analysis, postprocessing techniques.

1 Introduction

The Virtual Element Method (VEM) is a novel technique used for the numerical approximation of partial differential equations, which was originally introduced in [3], and later extended in [10] to handle mixed methods. Its applications to fluid mechanics has become a very active research subject in recent years. Indeed, regarding the Stokes equations, we can cite to [2, 16, 6, 12, 14, 28]. The Brinkman model has been addressed in [13, 32, 23], whereas VEM-discretizations for the Navier-Stokes equations have been developed in [7, 24, 27, 26]. Recently, a mixed-VEM for the Boussinesq problem has been proposed in [25].

The main motivation to use VEM is to construct Galerkin schemes with the capability to use general polygonal/polyhedral meshes, naturally including hanging nodes and non-convex shapes. In this way, the VEM approach offers several advantages due to the flexibility allowed to deal with general meshes. On one hand, this flexibility ensures that adaptive strategies can be implemented very easily and efficiently. On the other hand, the use of hanging nodes introduced by the refinement of a neighbouring element are simply treated as new nodes, which has been proved does not affect the quality of the approximation [15]. Thereby, local refinements can be performed on polygonal/polyhedral meshes

*CI^{2}MA and Departamento de Ingeniería Matemática, Universidad de Concepción, Casilla 160-C, Concepción, Chile, email: mmunar@ci2ma.udec.cl.

†Escuela de Matemática, Universidad Nacional, Campus Omar Dengo, Heredia, Costa Rica, email: filander.sequeira@una.cr.

using few elements, in contrast to classical mesh refinement techniques for triangular meshes, which suffer from the fact that local refinement propagates into neighbouring regions. Hence, the design and analysis of adaptive mesh refinement strategies based on a posteriori error indicators for the VEM approach and particularly for the mixed-VEM is an attractive task. However, the literature on a posteriori analysis for VEM is focused on primal schemes. In this regard, we can mention the following works [8, 15, 9, 29, 30, 18]. In particular, the authors of [8] proposed a posteriori error bounds for the C^1-conforming VEM for the two-dimensional Poisson problem. Next, a posteriori error bounds for the C^0-conforming VEM for the discretization of second-order linear elliptic reaction-convection-diffusion problems with nonconstant coefficients in two and three dimensions were proposed in [15], whereas a residual-based a posteriori error estimator for the VEM discretization of the Poisson problem with discontinuous diffusivity coefficient was introduced and analyzed in [9]. Moreover, in [29] and [30], the authors developed an a posteriori error analysis of a VEM approach for the Steklov eigenvalue problem and the spectral analysis for the elasticity equations, respectively. Finally, in [18] a general recovery-based a posteriori error estimation framework for the VEM of arbitrary order on general polygonal/polyhedral meshes has been developed.

On the other hand, in the context of mixed methods using the VEM approach, an a posteriori error analysis was recently developed in [17], applied to second order elliptic equations in divergence form with mixed boundary conditions. More precisely, the authors propose a framework to incorporate adaptive strategies to mixed-VEM on polygonal meshes. They employed techniques based in Helmholtz decomposition, local approximation properties of interpolation operators, inverse inequalities and localization arguments based on bubble functions, to construct a posteriori error estimates.

According to the above discussion, the main purpose of the present work is to apply the approach from [17] to develop an a posteriori error analysis and the corresponding adaptive strategy for the nonlinear Brinkman model of porous media flow proposed in [23]. To this end, we propose a residual-type estimator, which involves fully computable approximations of the pseudostress variable. The behavior of our estimator is analyzed with several numerical tests. The remainder of this paper is organized as follows. In Section 2 we introduce the model problem, the associated variational formulation and its respective mixed virtual element scheme. The a posteriori error analysis of our method, which constitutes the main contribution of this work, is presented in details in Section 3. Finally, we propose an adaptive algorithm and validate its effectiveness with some numerical examples in Section 4.

We end this section with several notations to be used throughout the paper. Firstly, we let $\mathbb{I}$ be the identity matrix in $\mathrm{R}^{2\times 2}$, and for any $\boldsymbol{\tau} := (\tau_{ij})$, $\boldsymbol{\zeta} := (\zeta_{ij}) \in \mathrm{R}^{2\times 2}$, we set

$$\boldsymbol{\tau}^{\mathbf{t}} \;:=\; (\tau_{ji})\,, \quad \mathrm{tr}(\boldsymbol{\tau}) \;:=\; \sum_{i=1}^{2} \tau_{ii}, \quad \boldsymbol{\tau}^{\mathbf{d}} \;:=\; \boldsymbol{\tau} - \frac{1}{2}\,\mathrm{tr}(\boldsymbol{\tau})\,\mathbb{I} \quad \text{and} \quad \boldsymbol{\tau} : \boldsymbol{\zeta} \;:=\; \sum_{i,j=1}^{2} \tau_{ij}\zeta_{ij}\,,$$

which denote, respectively, the transpose, the trace, the deviator of the tensor $\boldsymbol{\tau}$, and the tensorial product between $\boldsymbol{\tau}$ and $\boldsymbol{\zeta}$. Next, given a bounded domain $\mathcal{O} \subseteq \mathrm{R}^2$, with polygonal boundary $\partial\mathcal{O}$, we utilize standard notations for Lebesgue spaces $\mathrm{L}^p(\mathcal{O})$, $p > 1$, and Sobolev spaces $\mathrm{H}^s(\mathcal{O})$, $s \in \mathrm{R}$, with norm $\|\cdot\|_{s,\mathcal{O}}$ and seminorm $|\cdot|_{s,\mathcal{O}}$. In particular, $\mathrm{H}^{1/2}(\partial\mathcal{O})$ is the space of traces of functions of $\mathrm{H}^1(\mathcal{O})$ and $\mathrm{H}^{-1/2}(\partial\mathcal{O})$ denotes its dual. Moreover, by $\mathbf{M}$ and $\mathbb{M}$ we will refer to the corresponding vector and tensorial counterparts of the generic scalar functional space M, and $\|\cdot\|$, with no subscripts, will stand for the natural norm of either an element or an operator in any product functional space. Furthermore, we recall that

$$\mathbb{H}(\mathbf{div};\mathcal{O}) \;:=\; \big\{\boldsymbol{\tau} \in \mathbb{L}^2(\mathcal{O}) : \quad \mathbf{div}(\boldsymbol{\tau}) \in \mathbf{L}^2(\mathcal{O})\big\}\,,$$

and

$$\mathbb{H}(\mathbf{rot};\mathcal{O}) \;:=\; \big\{\boldsymbol{\tau} \in \mathbb{L}^2(\mathcal{O}) : \quad \mathbf{rot}(\boldsymbol{\tau}) \in \mathbf{L}^2(\mathcal{O})\big\}\,,$$

equipped with the usual norms

$$\|\boldsymbol{\tau}\|^2_{\mathbf{div};\mathcal{O}} \;:=\; \|\boldsymbol{\tau}\|^2_{0,\mathcal{O}} \,+\, \|\mathbf{div}(\boldsymbol{\tau})\|^2_{0,\mathcal{O}} \qquad \forall\, \boldsymbol{\tau} \in \mathbb{H}(\mathbf{div};\mathcal{O})\,,$$

and

$$\|\boldsymbol{\tau}\|^2_{\mathbf{rot};\mathcal{O}} \;:=\; \|\boldsymbol{\tau}\|^2_{0,\mathcal{O}} \,+\, \|\mathbf{rot}(\boldsymbol{\tau})\|^2_{0,\mathcal{O}} \qquad \forall\, \boldsymbol{\tau} \in \mathbb{H}(\mathbf{rot};\mathcal{O})\,,$$

are Hilbert space. Also, we define

$$\mathbb{L}^2_{\mathrm{tr}}(\mathcal{O}) \;:=\; \big\{\mathbf{s} \in \mathbb{L}^2(\mathcal{O}) : \quad \mathrm{tr}(\mathbf{s}) = 0\big\}\,, \tag{1.1}$$

and

$$\mathbb{H}_0(\mathbf{div};\mathcal{O}) \;:=\; \left\{\boldsymbol{\tau} \in \mathbb{H}(\mathbf{div};\mathcal{O}) : \quad \int_{\mathcal{O}} \mathrm{tr}(\boldsymbol{\tau}) = 0\right\}\,. \tag{1.2}$$

Furthermore, we recall (see [11, 19]) that there holds the decomposition

$$\mathbb{H}(\mathbf{div};\mathcal{O}) \;=\; \mathbb{H}_0(\mathbf{div};\mathcal{O}) \oplus \mathrm{R}\,\mathbb{I}\,, \tag{1.3}$$

which, for each $\boldsymbol{\tau} \in \mathbb{H}(\mathbf{div};\mathcal{O})$ indicates that there exist unique $\boldsymbol{\tau}_0 \in \mathbb{H}_0(\mathbf{div};\mathcal{O})$ and $c := \frac{1}{2|\mathcal{O}|}\int_{\mathcal{O}} \mathrm{tr}(\boldsymbol{\tau})$ $\in \mathrm{R}$, where $|\mathcal{O}|$ denotes the measure of $\mathcal{O}$, such that $\boldsymbol{\tau} = \boldsymbol{\tau}_0 + c\,\mathbb{I}$. Finally, we employ $\mathbf{0}$ to denote a generic null vector, null tensor or null operator, and use C and c, with or without subscripts to denote generic constants independent of the discretization parameters, which may take different values at different places.

2 The nonlinear Brinkman model

In this section we briefly describe the augmented formulation considered in this work for the nonlinear Brinkman model. Firstly, in Section 2.1 we recall the system of partial differential equations modeling the problem, and its corresponding variational formulation. Then, the mixed-VEM discretization is discussed in Section 2.2.

2.1 The model problem and its continuous formulation

Let $\Omega \subseteq \mathrm{R}^2$ be a bounded domain with polygonal boundary Γ. Then, a nonlinear Brinkman model of porous media flow is given by the following system of partial differential equations

$$\begin{aligned} &\boldsymbol{\sigma} \;=\; \mu(|\nabla\mathbf{u}|)\nabla\mathbf{u} - p\,\mathbb{I} \quad \text{in} \quad \Omega\,, \qquad \alpha\mathbf{u} \,-\, \mathbf{div}(\boldsymbol{\sigma}) \;=\; \mathbf{f} \quad \text{in} \quad \Omega\,,\\ &\mathrm{div}(\mathbf{u}) \;=\; 0 \quad \text{in} \quad \Omega\,, \qquad \mathbf{u} \;=\; \mathbf{g} \quad \text{on} \quad \Gamma \qquad \text{and} \qquad \int_\Omega p \;=\; 0\,, \end{aligned} \tag{2.1}$$

where the unknowns are given by the pseudostress $\boldsymbol{\sigma}$, the velocity $\mathbf{u}$ and the pressure p of a fluid occupying the region Ω. The nonlinear function $\mu : \mathrm{R}^+ \to \mathrm{R}$ represents the kinematic viscosity function of the fluid, $\alpha > 0$ is a constant approximation of the viscosity divided by the permeability, $\mathbf{f} \in \mathbf{L}^2(\Omega)$, and $\mathbf{g} \in \mathbf{H}^{1/2}(\Gamma)$ is a boundary data. Notice that the data $\mathbf{g}$ must satisfy the compatibility condition $\int_\Gamma \mathbf{g}\cdot\boldsymbol{\nu} = 0$, where $\boldsymbol{\nu}$ is the unit outward normal on Γ, whereas the uniqueness of a pressure solution is ensured by the last equation of (2.1).

In what follows, we let $\psi_{ij} : \mathrm{R}^{2\times2} \to \mathrm{R}$ be the mapping given by $\psi_{ij}(\mathbf{r}) := \mu(|\mathbf{r}|)r_{ij}$ for each $\mathbf{r} := (r_{ij}) \in \mathrm{R}^{2\times2}$. Then, throughout this paper we assume that μ is of class C^1 and that there exist $\gamma_0, \alpha_0 > 0$ such that for each $\mathbf{r} := (r_{ij}), \mathbf{s} := (s_{ij}) \in \mathrm{R}^{2\times2}$, there hold

$$|\psi_{ij}(\mathbf{r})| \;\le\; \gamma_0\,|\mathbf{r}|\,, \qquad \left|\frac{\partial}{\partial r_{kl}}\psi_{ij}(\mathbf{r})\right| \;\le\; \gamma_0 \qquad \forall\, i,j,k,l \in \{1,2\}\,,$$

and

$$\sum_{i,j,k,l=1}^{2} \frac{\partial}{\partial r_{kl}} \psi_{ij}(\mathbf{r}) s_{ij} s_{kl} \;\geq\; \alpha_0 \, |\mathbf{s}|^2 .$$

We recall here that the assumptions above allow us to define a nonlinear operator $\mathbb{A} : \mathbb{L}^2(\Omega) \to [\mathbb{L}^2(\Omega)]'$ given by

$$[\mathbb{A}(\mathbf{r}), \mathbf{s}] \;:=\; \int_\Omega \boldsymbol{\psi}(\mathbf{r}) : \mathbf{s} \;=\; \int_\Omega \mu(|\mathbf{r}|)\mathbf{r} : \mathbf{s} \qquad \forall\, \mathbf{r}, \mathbf{s} \in \mathbb{L}^2(\Omega)\,, \tag{2.2}$$

which is Lipschitz-continuous and strongly monotone (cf. [22, Lemma 2.1]). More precisely, there hold

$$\|\mathbb{A}(\mathbf{r}) - \mathbb{A}(\mathbf{s})\|_{[\mathbb{L}^2(\Omega)]'} \;\leq\; \gamma_0 \|\mathbf{r} - \mathbf{s}\|_{0,\Omega} \qquad \text{and} \qquad [\mathbb{A}(\mathbf{r}) - \mathbb{A}(\mathbf{s}), \mathbf{r} - \mathbf{s}] \;\geq\; \alpha_0 \|\mathbf{r} - \mathbf{s}\|_{0,\Omega}^2\,, \tag{2.3}$$

for each $\mathbf{r}, \mathbf{s} \in \mathbb{L}^2(\Omega)$.

Now, as was explained in [20], using the incompressibility condition to eliminate the pressure, and introducing the auxiliary unknown $\mathbf{t} := \nabla \mathbf{u}$ in Ω, we can rewrite (2.1) as follows:

$$\begin{gathered} \mathbf{t} \;=\; \nabla \mathbf{u} \quad \text{in} \quad \Omega, \qquad \boldsymbol{\sigma}^{\mathbf{d}} \;=\; \mu(|\mathbf{t}|)\mathbf{t} \quad \text{in} \quad \Omega\,, \qquad \alpha \mathbf{u} - \mathbf{div}(\boldsymbol{\sigma}) \;=\; \mathbf{f} \quad \text{in} \quad \Omega\,, \\ \operatorname{tr}(\mathbf{t}) \;=\; 0 \quad \text{in} \quad \Omega\,, \qquad \mathbf{u} \;=\; \mathbf{g} \quad \text{on} \quad \Gamma \qquad \text{and} \qquad \int_\Omega \operatorname{tr}(\boldsymbol{\sigma}) \;=\; 0\,. \end{gathered} \tag{2.4}$$

We recall that the pressure can be obtained using the formula (cf. [23, Section 2.2])

$$p \;=\; -\frac{1}{2} \operatorname{tr}(\boldsymbol{\sigma}) \quad \text{in} \quad \Omega\,. \tag{2.5}$$

Note from the fourth and last equation of (2.4) that $\mathbf{t}$ and $\boldsymbol{\sigma}$ must belong to $\mathbb{L}^2_{\mathrm{tr}}(\Omega)$ (cf. (1.1)) and $\mathbb{H}_0(\mathbf{div};\Omega)$ (cf. (1.2)), respectively. In what follows, we make use of the notation $X := \mathbb{L}^2_{\mathrm{tr}}(\Omega)$ and $H := \mathbb{H}_0(\mathbf{div};\Omega)$. Then, proceeding as in [23, Section 2.2], that is, testing the first two equations of (2.4) by suitable test functions, integrating by parts, using the Dirichlet conditions for $\mathbf{u}$, the fact that the velocity can be replaced from the third equation of (2.4) as $\mathbf{u} = \frac{1}{\alpha}\big\{\mathbf{f} + \mathbf{div}(\boldsymbol{\sigma})\big\}$, and adding the following redundant term

$$\kappa \int_\Omega \big\{\boldsymbol{\sigma}^{\mathbf{d}} - \mu(|\mathbf{t}|)\mathbf{t}\big\} : \boldsymbol{\tau}^{\mathbf{d}} \;=\; 0 \qquad \forall\, \boldsymbol{\tau} \in H\,,$$

with κ a positive parameter to be specified later, we arrive at the augmented variational formulation: Find $(\mathbf{t}, \boldsymbol{\sigma}) \in X \times H$ such that

$$[\mathbf{A}(\mathbf{t}, \boldsymbol{\sigma}), (\mathbf{s}, \boldsymbol{\tau})] \;=\; [\mathbf{F}, (\mathbf{s}, \boldsymbol{\tau})] \qquad \forall\, (\mathbf{s}, \boldsymbol{\tau}) \in X \times H\,, \tag{2.6}$$

where $\mathbf{A} : X \times H \to (X \times H)'$ and $\mathbf{F} : X \times H \to \mathrm{R}$ are given by

$$\begin{aligned} [\mathbf{A}(\mathbf{t}, \boldsymbol{\sigma}), (\mathbf{s}, \boldsymbol{\tau})] \;\;:=\;\; & [\mathbb{A}(\mathbf{t}), \mathbf{s} - \kappa \boldsymbol{\tau}^{\mathbf{d}}] \;-\; \int_\Omega \mathbf{s} : \boldsymbol{\sigma}^{\mathbf{d}} \;+\; \int_\Omega \mathbf{t} : \boldsymbol{\tau}^{\mathbf{d}} \;+\; \kappa \int_\Omega \boldsymbol{\sigma}^{\mathbf{d}} : \boldsymbol{\tau}^{\mathbf{d}} \\ & + \frac{1}{\alpha} \int_\Omega \mathbf{div}(\boldsymbol{\sigma}) \cdot \mathbf{div}(\boldsymbol{\tau})\,, \end{aligned} \tag{2.7}$$

and

$$[\mathbf{F}, (\mathbf{s}, \boldsymbol{\tau})] \;:=\; -\frac{1}{\alpha} \int_\Omega \mathbf{f} \cdot \mathbf{div}(\boldsymbol{\tau}) \;+\; \langle \boldsymbol{\tau\nu}, \mathbf{g} \rangle\,, \tag{2.8}$$

respectively, where $\langle \cdot, \cdot \rangle$ stands for the duality pairing between $\mathbf{H}^{-1/2}(\Gamma)$ and $\mathbf{H}^{1/2}(\Gamma)$.

In addition, the analysis of the continuous formulation (2.6) is based in results of nonlinear analysis (cf. [23, Section 2.2]). More precisely, it was proved there the Lipschitz-continuity of the operator $\mathbf{A}$, that is, there exists $L_{\mathbf{A}} > 0$ (cf [23, eq. 2.18]), depending only on κ, γ_0 and α, such that

$$\|\mathbf{A}(\mathbf{r},\boldsymbol{\zeta}) - \mathbf{A}(\mathbf{s},\boldsymbol{\tau})\|_{(X\times H)'} \;\leq\; L_{\mathbf{A}}\,\|(\mathbf{r},\boldsymbol{\zeta}) - (\mathbf{s},\boldsymbol{\tau})\|_{X\times H}\,, \qquad \forall\,(\mathbf{r},\boldsymbol{\zeta}),\,(\mathbf{s},\boldsymbol{\tau}) \in X\times H\,. \tag{2.9}$$

Furthermore, for $\kappa \in \left(0, \frac{2\delta\alpha_0}{\gamma_0}\right)$ with $\delta \in \left(0, \frac{2}{\gamma_0}\right)$ there exists $C_{SM} > 0$ (cf. [23, Lemma 2.2]), depending only on $\kappa, \alpha_0, \gamma_0, \delta, \Omega$ and α, such that

$$[\mathbf{A}(\mathbf{r},\boldsymbol{\zeta}) - \mathbf{A}(\mathbf{s},\boldsymbol{\tau}), (\mathbf{r},\boldsymbol{\zeta}) - (\mathbf{s},\boldsymbol{\tau})] \;\geq\; C_{SM}\|(\mathbf{r},\boldsymbol{\zeta}) - (\mathbf{s},\boldsymbol{\tau})\|^2_{X\times H} \qquad \forall\,(\mathbf{r},\boldsymbol{\zeta}),(\mathbf{s},\boldsymbol{\tau}) \in X\times H\,,$$

which yielded the strong monotonicity of the operator $\mathbf{A}$. In this way, the well-posedness of the variational formulation (2.6) is established by the following theorem.

Theorem 2.1. Assume that $\mathbf{f} \in \mathbf{L}^2(\Omega), \mathbf{g} \in \mathbf{H}^{1/2}(\Gamma)$, and that given $\delta \in \left(0, \frac{2}{\gamma_0}\right)$, the parameter κ lies in $\left(0, \frac{2\delta\alpha_0}{\gamma_0}\right)$. Then, there exists a unique $(\mathbf{t},\boldsymbol{\sigma}) \in X\times H$ solution of (2.6). Moreover, there exists a positive constant C, depending only on $\Omega, \alpha_0, \gamma_0, \kappa$ and α, such that

$$\|(\mathbf{t},\boldsymbol{\sigma})\|_{X\times H} \;\leq\; C\big\{\|\mathbf{f}\|_{0,\Omega} \;+\; \|\mathbf{g}\|_{1/2,\Gamma}\big\}.$$

Proof. See [23, Theorem 2.1]). □

2.2 The mixed virtual element method

Regarding the mesh, given $\{\mathcal{T}_h\}_{h>0}$ a family of partitions of Ω into an open non-overlapping polygonal elements and $K \in \mathcal{T}_h$, we denote its barycenter, diameter and number of edges by $\mathbf{x}_K$, h_K, and d_K, respectively, and define, as usual, $h := \max\{h_K : K \in \mathcal{T}_h\}$. In addition, in what follows we assume that there exists a constant $C_{\mathcal{T}} > 0$ such that for each partition $\mathcal{T}_h$ and for each $K \in \mathcal{T}_h$ there hold:

a) the ratio between the shortest edge and the diameter h_K of K is bigger than $C_{\mathcal{T}}$, and

b) K is star-shaped with respect to a ball B of radius $C_{\mathcal{T}} h_K$ and center $\mathbf{x}_B \in K$.

We recall here, from the above assumptions, that it is possible to show that each $K \in \mathcal{T}_h$ is simply connected, and that there exists an integer $N_{\mathcal{T}}$ (depending only on $C_{\mathcal{T}}$), such that the numbers of edges of each $K \in \mathcal{T}_h$ is bounded above by $N_{\mathcal{T}}$. Furthermore, the assumption b) implies that each element K admits a sub-triangulation $\mathcal{T}_h^K$, obtained by joining each vertex of K with the point with respect to which K is starred. In this way, since we are also assuming a), we have that the resulting global triangulation $\widehat{\mathcal{T}_h} := \displaystyle\bigcup_{K\in\mathcal{T}_h} \mathcal{T}_h^K$ is shape regular. Finally, partitions including non-convex elements are allowed, as also meshes with hanging nodes.

Now, given an integer $\ell \geq 0$ and $\mathcal{O} \subseteq \mathrm{R}^2$, we let $\mathrm{P}_\ell(\mathcal{O})$ be the space of polynomials on $\mathcal{O}$ of degree up to ℓ, and according to Section 1, we set $\mathbf{P}_\ell(\mathcal{O}) := [\mathrm{P}_\ell(\mathcal{O})]^2$ and $\mathbb{P}_\ell(\mathcal{O}) := [\mathrm{P}_\ell(\mathcal{O})]^{2\times 2}$. In addition, given an edge e of $\mathcal{T}_h$ with barycenter x_e and diameter h_e, we introduce the following set of $(\ell+1)$ normalized monomials on e

$$\mathcal{B}_\ell(e) \;:=\; \left\{\left(\frac{x - x_e}{h_e}\right)^j\right\}_{0\leq j\leq \ell}\,,$$

which certainly constitutes a basis on $\mathrm{P}_\ell(e)$. Similarly, given $K \in \mathcal{T}_h$ with barycenter $\mathbf{x}_K$, we define the following set of $\frac{1}{2}(\ell+1)(\ell+2)$ normalized monomials

$$\mathcal{B}_\ell(K) \;:=\; \left\{\left(\frac{\mathbf{x} - \mathbf{x}_K}{h_K}\right)^{\boldsymbol{\alpha}}\right\}_{0\leq |\boldsymbol{\alpha}|\leq \ell}\,,$$

which is a basis of $\mathrm{P}_\ell(K)$. Notice that in the definition of $\mathcal{B}_\ell(K)$ above, we have made use of the multi-index notation, that is, given $\mathbf{x} := (x_1, x_2)^{\mathbf{t}} \in \mathrm{R}^2$ and $\boldsymbol{\alpha} := (\alpha_1, \alpha_2)^{\mathbf{t}}$, with non-negative integers α_1, α_2, we set $\mathbf{x}^{\boldsymbol{\alpha}} := x_1^{\alpha_1} x_2^{\alpha_2}$ and $|\boldsymbol{\alpha}| := \alpha_1 + \alpha_2$. Furthermore, for e and K as indicated, we define

$$\boldsymbol{\mathcal{B}}_\ell(e) \;:=\; \big\{(q,0)^{\mathbf{t}} : \quad q \in \mathcal{B}_\ell(e)\big\} \cup \big\{(0,q)^{\mathbf{t}} : \quad q \in \mathcal{B}_\ell(e)\big\}\,,$$

and

$$\boldsymbol{\mathcal{B}}_\ell(K) \;:=\; \big\{(q,0)^{\mathbf{t}} \;: \quad q \in \mathcal{B}_\ell(K)\big\} \cup \big\{(0,q)^{\mathbf{t}} : \quad q \in \mathcal{B}_\ell(K)\big\}\,.$$

In addition, for each integer $\ell \geq 0$, we let $\mathcal{G}_\ell(K)$ be a basis of $\big(\nabla \mathrm{P}_{\ell+1}(K)\big)^\perp \cap \mathbf{P}_\ell(K)$, which is the $\mathbf{L}^2(K)$-orthogonal of $\nabla \mathrm{P}_{\ell+1}(K)$ in $\mathbf{P}_\ell(K)$, and denote its tensorial counterpart as follows:

$$\boldsymbol{\mathcal{G}}_\ell(K) \;:=\; \left\{\begin{pmatrix}\mathbf{q}^{\mathbf{t}}\\ \mathbf{0}\end{pmatrix} : \quad \mathbf{q} \in \mathcal{G}_\ell(K)\right\} \cup \left\{\begin{pmatrix}\mathbf{0}\\ \mathbf{q}^{\mathbf{t}}\end{pmatrix} : \quad \mathbf{q} \in \mathcal{G}_\ell(K)\right\}.$$

We remark that, alternatively, one could also consider another choices, not necessarily orthogonal, that have been proposed recently, such as $\mathbf{P}_k(K) = \nabla \mathrm{P}_{k+1} \oplus \mathbf{x}^\perp \mathrm{P}_{k-1}(K)$, where, given $\mathbf{x} := (x_1, x_2)^{\mathbf{t}} \in \mathrm{R}^2$, $\mathbf{x}^\perp$ denotes the rotated vector $(-x_2, x_1)^{\mathbf{t}}$. Actually, it is not difficult to see that it suffices to choose any space $\mathcal{G}(K)$ such that $\mathbf{P}_\ell(K) = \nabla \mathrm{P}_{\ell+1} \oplus \mathcal{G}(K)$.

Throughout the paper, we denote by $\mathcal{P}_k^K : \mathbf{L}^2(K) \to \mathbf{P}_k(K)$ the $\mathbf{L}^2(K)$-orthogonal projection onto the space $\mathbf{P}_k(K)$, for any $K \in \mathcal{T}_h$ and $k \geq 0$. In addition, we will make use of a tensorial version of the aforementioned projector, which is denoted by $\boldsymbol{\mathcal{P}}_k^K$. The following approximation properties of these projectors are well-known:

$$\|\mathbf{v} - \mathcal{P}_k^K(\mathbf{v})\|_{0,K} \;\leq\; C h_K^s |\mathbf{v}|_{s,K} \qquad \text{and} \qquad \|\boldsymbol{\zeta} - \boldsymbol{\mathcal{P}}_k^K(\boldsymbol{\zeta})\|_{0,K} \leq C h_K^s |\boldsymbol{\zeta}|_{s,K} \tag{2.10}$$

for all $K \in \mathcal{T}_h$, and for all $\mathbf{v} \in \mathbf{H}^s(K), \boldsymbol{\zeta} \in \mathbb{H}^s(K)$ with $s \in \{0, \ldots, k+1\}$. Finally, we now denote by $\mathcal{P}_k^h$ and $\boldsymbol{\mathcal{P}}_k^h$, respectively, their global counterparts, that is, given $\mathbf{v} \in \mathbf{L}^2(\Omega)$ and $\boldsymbol{\zeta} \in \mathbb{L}^2(\Omega)$, we let

$$\mathcal{P}_k^h(\mathbf{v})\big|_K \;:=\; \mathcal{P}_k^K(\mathbf{v}\big|_K) \qquad \text{and} \qquad \boldsymbol{\mathcal{P}}_k^h(\boldsymbol{\zeta})\big|_K \;:=\; \boldsymbol{\mathcal{P}}_k^K(\boldsymbol{\zeta}\big|_K) \qquad \forall\, K \in \mathcal{T}_h\,.$$

2.2.1 The virtual element space and its approximation properties

Let $k \geq 0$ be an integer. Then, we define the finite dimensional subspaces of X and H, respectively, as

$$X_k^h \;:=\; \Big\{\mathbf{s} \in X : \quad \mathbf{s}\big|_K \in X_k^K \quad \forall\, K \in \mathcal{T}_h\Big\} \tag{2.11}$$

and

$$H_k^h \;:=\; \Big\{\boldsymbol{\tau} \in H : \quad \boldsymbol{\tau}\big|_K \in H_k^K \quad \forall\, K \in \mathcal{T}_h\Big\}\,, \tag{2.12}$$

where, given $K \in \mathcal{T}_h$, $X_k^K := \mathbb{P}_k(K)$ and H_k^K is the space introduced in [5, Section 3.1], given by

$$\begin{aligned} H_k^K \;:=\; \big\{\boldsymbol{\tau} \in \mathbb{H}(\mathbf{div}; K) \cap \mathbb{H}(\mathbf{rot}; K) : &\quad \boldsymbol{\tau}\boldsymbol{\nu}|_e \in \mathbf{P}_k(e) \quad \forall \text{ edge } e \in \partial K\,, \\ \mathbf{div}(\boldsymbol{\tau}) \in \mathbf{P}_k(K) &\quad \text{and} \quad \mathbf{rot}(\boldsymbol{\tau}) \in \mathbf{P}_{k-1}(K)\big\}\,. \end{aligned} \tag{2.13}$$

The degrees of freedom guaranteeing unisolvency for each $\boldsymbol{\tau} \in H_k^K$ are defined by (see, e.g., [4], [5])

$$\begin{aligned} &\int_e \boldsymbol{\tau}\boldsymbol{\nu} \cdot \mathbf{q} && \forall\, \mathbf{q} \in \boldsymbol{\mathcal{B}}_k(e)\,, \quad \forall \text{ edge } e \in \partial K\,, \\ &\int_K \boldsymbol{\tau} : \nabla \mathbf{p} && \forall\, \mathbf{p} \in \boldsymbol{\mathcal{B}}_k(K) \setminus \{(1,0)^{\mathbf{t}}, (0,1)^{\mathbf{t}}\}\,, \\ &\int_K \boldsymbol{\tau} : \boldsymbol{\rho} && \forall\, \boldsymbol{\rho} \in \boldsymbol{\mathcal{G}}_k(K)\,. \end{aligned} \tag{2.14}$$

We now introduce the interpolation operator $\mathbf{\Pi}_k^K : \mathbb{H}^1(K) \to H_k^K$, which is defined for each $\boldsymbol{\tau} \in \mathbb{H}^1(K)$ as the unique $\mathbf{\Pi}_k^K(\boldsymbol{\tau})$ in H_k^K such that

$$\begin{aligned}
\int_e (\boldsymbol{\tau} - \mathbf{\Pi}_k^K(\boldsymbol{\tau}))\boldsymbol{\nu} \cdot \mathbf{q} &= 0 \qquad \forall\, \mathbf{q} \in \boldsymbol{\mathcal{B}}_k(e)\,, \quad \forall \text{ edge } e \in \partial K\,,\\
\int_K (\boldsymbol{\tau} - \mathbf{\Pi}_k^K(\boldsymbol{\tau})) : \nabla \mathbf{p} &= 0 \qquad \forall\, \mathbf{p} \in \boldsymbol{\mathcal{B}}_k(K) \setminus \{(1,0)^{\mathbf{t}}, (0,1)^{\mathbf{t}}\}\,,\\
\int_K (\boldsymbol{\tau} - \mathbf{\Pi}_k^K(\boldsymbol{\tau})) : \boldsymbol{\rho} &= 0 \qquad \forall\, \boldsymbol{\rho} \in \boldsymbol{\mathcal{G}}_k(K)\,.
\end{aligned} \tag{2.15}$$

Concerning the approximation properties of $\mathbf{\Pi}_k^K$, we first recall from [5, eq. 3.19] that for each $\boldsymbol{\tau} \in \mathbb{H}^s(K)$, with $s \in \big\{1, \ldots, k+1\big\}$, there holds

$$\|\boldsymbol{\tau} - \mathbf{\Pi}_k^K(\boldsymbol{\tau})\|_{0,K} \;\le\; C\, h_K^s\, |\boldsymbol{\tau}|_{s,K}\,. \tag{2.16}$$

Now, from (2.10) and the following conmutative property

$$\mathbf{div}(\mathbf{\Pi}_k^K(\boldsymbol{\tau})) \;=\; \mathcal{P}_k^K(\mathbf{div}(\boldsymbol{\tau})) \qquad \forall\, \boldsymbol{\tau} \in \mathbb{H}^1(K)\,, \tag{2.17}$$

we deduce, for each $\boldsymbol{\tau} \in \mathbb{H}^1(K)$ such that $\mathbf{div}(\boldsymbol{\tau}) \in \mathbf{H}^s(K)$, with $s \in \big\{0, \ldots, k+1\big\}$, that there holds

$$\|\mathbf{div}(\boldsymbol{\tau}) - \mathbf{div}(\mathbf{\Pi}_k^K(\boldsymbol{\tau}))\|_{0,K} \;\le\; C\, h_K^s\, |\mathbf{div}(\boldsymbol{\tau})|_{s,K}\,. \tag{2.18}$$

In addition (cf. [17, Lemma 5.2]), for each $\boldsymbol{\tau} \in \mathbb{H}^1(\Omega)$ there holds

$$\|\boldsymbol{\tau}\boldsymbol{\nu} - \mathbf{\Pi}_k^K(\boldsymbol{\tau})\boldsymbol{\nu}\|_{0,e} \le C\, h_e^{1/2} \|\boldsymbol{\tau}\|_{1,K} \qquad \forall \text{ edge } e \in \mathcal{T}_h\,, \tag{2.19}$$

where K is any element of $\mathcal{T}_h$ such that e is an edge of K.

2.2.2 The discrete scheme and a priori error estimates

We now recall the discrete formulation proposed in [23, Section 3.3]. Indeed, using the fact that the degrees of freedom introduced in (2.14) allow us the explicit computation of the orthogonal projection on $\mathbb{P}_k(K)$ for each $\boldsymbol{\tau} \in H_k^K$ (cf. [5, Section 3.2]), we define the local discrete nonlinear operator $\mathbf{A}_h^K : (X_k^K \times H_k^K) \to (X_k^K \times H_k^K)'$ given by

$$\begin{aligned}
[\mathbf{A}_h^K(\mathbf{r}, \boldsymbol{\zeta}), (\mathbf{s}, \boldsymbol{\tau})] \;:=\; & [\mathbb{A}(\mathbf{r}), \mathbf{s} - \kappa(\boldsymbol{\mathcal{P}}_k^K(\boldsymbol{\tau}))^{\mathbf{d}}] - \int_K (\boldsymbol{\mathcal{P}}_k^K(\boldsymbol{\zeta}))^{\mathbf{d}} : \mathbf{s} + \int_K (\boldsymbol{\mathcal{P}}_k^K(\boldsymbol{\tau}))^{\mathbf{d}} : \mathbf{r}\\
& + \kappa \int_K (\boldsymbol{\mathcal{P}}_k^K(\boldsymbol{\zeta}))^{\mathbf{d}} : (\boldsymbol{\mathcal{P}}_k^K(\boldsymbol{\tau}))^{\mathbf{d}} + \frac{1}{\alpha} \int_K \mathbf{div}(\boldsymbol{\zeta}) \cdot \mathbf{div}(\boldsymbol{\tau})\\
& + \mathcal{S}^K(\boldsymbol{\zeta} - \boldsymbol{\mathcal{P}}_k^K(\boldsymbol{\zeta}), \boldsymbol{\tau} - \boldsymbol{\mathcal{P}}_k^K(\boldsymbol{\tau}))
\end{aligned} \tag{2.20}$$

for all $(\mathbf{r}, \boldsymbol{\zeta}), (\mathbf{s}, \boldsymbol{\tau}) \in X_k^K \times H_k^K$, where $\mathcal{S}^K : H_k^K \times H_k^K \to \mathrm{R}$ is any symmetric and positive bilinear form verifying (see [3, Section 4.6] or [5, Section 3.3])

$$\widehat{c}_0 \|\boldsymbol{\zeta}\|_{0,K}^2 \;\le\; \mathcal{S}^K(\boldsymbol{\zeta}, \boldsymbol{\zeta}) \;\le\; \widehat{c}_1 \|\boldsymbol{\zeta}\|_{0,K}^2 \qquad \forall\, \boldsymbol{\zeta} \in H_k^K, \tag{2.21}$$

with constants $\widehat{c}_0$, $\widehat{c}_1 > 0$ depending only on $C_{\mathcal{T}}$. More precisely, for the numerical results reported below in Section 4 we take $\mathcal{S}^K$ as:

$$\mathcal{S}^K(\boldsymbol{\zeta}, \boldsymbol{\tau}) \;:=\; \sum_{j=1}^{n_k^K} m_{j,K}(\boldsymbol{\zeta})\, m_{j,K}(\boldsymbol{\tau}) \qquad \forall\, (\boldsymbol{\zeta}, \boldsymbol{\tau}) \in H_k^K \times H_k^K\,.$$

where n_k^K denote the dimension of H_k^K and $m_{j,K}$, $j \in \{1, 2, \ldots, n_k^K\}$ collects the degrees of freedom given by (2.14). Then, according to (2.20), we now introduce the global discrete nonlinear operator $\mathbf{A}_h : (X_k^h \times H_k^h) \to (X_k^h \times H_k^h)'$ as:

$$[\mathbf{A}_h(\mathbf{r}, \boldsymbol{\zeta}), (\mathbf{s}, \boldsymbol{\tau})] \; := \; \sum_{K \in \mathcal{T}_h} [\mathbf{A}_h^K(\mathbf{r}, \boldsymbol{\zeta}), (\mathbf{s}, \boldsymbol{\tau})] \qquad \forall\, (\mathbf{r}, \boldsymbol{\zeta}), (\mathbf{s}, \boldsymbol{\tau}) \in X_k^h \times H_k^h \,. \tag{2.22}$$

Therefore, the mixed virtual element scheme associated with the augmented formulation (2.6) reads: Find $(\mathbf{t}_h, \boldsymbol{\sigma}_h) \in X_k^h \times H_k^h$ such that

$$[\mathbf{A}_h(\mathbf{t}_h, \boldsymbol{\sigma}_h), (\mathbf{s}_h, \boldsymbol{\tau}_h)] \; = \; [\mathbf{F}, (\mathbf{s}_h, \boldsymbol{\tau}_h)] \qquad \forall\, (\mathbf{s}_h, \boldsymbol{\tau}_h) \in X_k^h \times H_k^h \,. \tag{2.23}$$

The inconsistency between $\mathbf{A}$ and $\mathbf{A}_h$ is established by the following result.

Lemma 2.1. There exists a constant $C > 0$, depending only on κ and $\widehat{c}_1$ (cf. (2.21)), such that

$$\begin{aligned} &[\mathbf{A}_h(\mathbf{r}_h, \boldsymbol{\zeta}_h) - \mathbf{A}(\mathbf{r}_h, \boldsymbol{\zeta}_h), (\mathbf{s}_h, \boldsymbol{\tau}_h)] \\ &\qquad \le \; C \left\{ \|\boldsymbol{\zeta}_h - \boldsymbol{\mathcal{P}}_k^h(\boldsymbol{\zeta}_h)\|_{0,\Omega} \, + \, \|(\boldsymbol{\mathcal{P}}_k^h(\boldsymbol{\zeta}_h))^{\mathbf{d}} - \mu(|\mathbf{r}_h|)\, \mathbf{r}_h\|_{0,\Omega} \right\} \|(\mathbf{s}_h, \boldsymbol{\tau}_h)\|_{X \times H} \end{aligned}$$

for all $(\mathbf{r}_h, \boldsymbol{\zeta}_h), (\mathbf{s}_h, \boldsymbol{\tau}_h) \in X_k^h \times H_k^h$.

Proof. It is a light modification of [23, Lemma 4.1]. □

The unique solvability and stability of the virtual scheme (2.23) is established now.

Theorem 2.2. Assume that given $\delta \in \left(0, \frac{2}{\gamma_0}\right)$, the parameter κ lies in $\left(0, \frac{2\delta\alpha_0}{\gamma_0}\right)$. Then, there exists a unique $(\mathbf{t}_h, \boldsymbol{\sigma}_h) \in X_k^h \times H_k^h$ solution of (2.23), and there exists a positive constant C, independent of h, such that

$$\|(\mathbf{t}_h, \boldsymbol{\sigma}_h)\|_{X \times H} \; \le \; C \left\{ \|\mathbf{f}\|_{0,\Omega} \, + \, \|\mathbf{g}\|_{1/2,\Gamma} \right\}.$$

Proof. See [23, Theorem 3.1]. □

Now, we recall that the respective a priori error estimates for (2.6) and the corresponding rate of convergence was developed in [23, Section 4]. More precisely, we have the following result.

Theorem 2.3. Let $(\boldsymbol{\sigma}, \boldsymbol{\tau}) \in X \times H$ and $(\boldsymbol{\sigma}_h, \boldsymbol{\tau}_h) \in X_k^h \times H_h^h$ be the unique solutions of the continuous and discrete schemes (2.6) and (2.23), respetively. Assume that for some $s \in [1, k+1]$ there hold $\mathbf{t}\big|_K, \boldsymbol{\sigma}\big|_K \in \mathbb{H}^s(K)$, and $\mathbf{div}(\boldsymbol{\sigma}) \in \mathbf{H}^s(K)$ for each $K \in \mathcal{T}_h$. Then, there exists $C > 0$, independent of h, such that

$$\|\mathbf{t} - \mathbf{t}_h\|_X \, + \, \|\boldsymbol{\sigma} - \boldsymbol{\sigma}_h\|_H \; \le \; C h^s \sum_{K \in \mathcal{T}_h} \left\{ |\mathbf{t}|_{s,K} \, + \, |\boldsymbol{\sigma}|_{s,K} \, + \, |\mathbf{div}(\boldsymbol{\sigma})|_{s,K} \right\}.$$

Proof. See [23, Theorem 4.2]. □

Next, as usual in VEM discretizations it is neccesary to get error estimates for computable approximations of the virtual solution. To this end, we construct two approximations from the virtual solution $\boldsymbol{\sigma}_h$, which are computed locally. The first one is obtained as its $\mathbf{L}^2(\Omega)$-orthogonal projection on $\mathbb{P}_k(K)$, namely

$$\widehat{\boldsymbol{\sigma}}_{h,K} \; := \; \boldsymbol{\mathcal{P}}_k^K(\boldsymbol{\sigma}_h|_K) \qquad \forall\, K \in \mathcal{T}_h \,, \tag{2.24}$$

whereas the second one, which is denoted by $\boldsymbol{\sigma}_{h,K}^{\star}$ and belong to $\mathbb{P}_{k+1}(K)$, is computed as the unique solution of the local problem

$$(\boldsymbol{\sigma}_{h,K}^{\star}, \boldsymbol{\tau}_h)_{\mathbf{div};K} \;=\; \int_K \widehat{\boldsymbol{\sigma}}_{h,K} : \boldsymbol{\tau}_h \;+\; \int_K \mathbf{div}(\boldsymbol{\sigma}_h)\cdot\mathbf{div}(\boldsymbol{\tau}_h) \qquad \forall\, \boldsymbol{\tau}_h \in \mathbb{P}_{k+1}(K)\,, \tag{2.25}$$

where $(\cdot,\cdot)_{\mathbf{div};K}$ stands for the usual $\mathbb{H}(\mathbf{div};K)$-inner product induced by norm $\|\cdot\|_{\mathbf{div};K}$. We remark here that the two approximations of $\boldsymbol{\sigma}_h$ can be explicitly computed for each $K\in\mathcal{T}_h$ using only its degrees of freedom. For more details see [23, Section 4.3] or [13, Section 5.3].

In what follows, for the approximation $\widehat{\boldsymbol{\sigma}}_{h,K}$ introduced in (2.24), we denote by $\widehat{\boldsymbol{\sigma}}_h$ its global counterpart, that is, $\widehat{\boldsymbol{\sigma}}_h\big|_K := \widehat{\boldsymbol{\sigma}}_{h,K}$ for all $K\in\mathcal{T}_h$. In this way, the following theorems provide the theoretical rates of convergence for $\widehat{\boldsymbol{\sigma}}_h$, $\boldsymbol{\sigma}_{h,K}^{\star}$ and the postproccesing variables p_h and $\mathbf{u}_h$ (cf. [23, Section 4.1]), which are given by

$$p_h \;:=\; -\int_\Omega \operatorname{tr}(\widehat{\boldsymbol{\sigma}}_h) \qquad \text{and} \qquad \mathbf{u}_h \;:=\; \frac{1}{\alpha}\Big\{\mathcal{P}_k^h(\mathbf{f}) + \mathbf{div}(\boldsymbol{\sigma}_h)\Big\}\,. \tag{2.26}$$

Theorem 2.4. Let $(\mathbf{t},\boldsymbol{\sigma})\in X\times H$ and $(\mathbf{t}_h,\boldsymbol{\sigma}_h)\in X_k^h\times H_k^h$ be the unique solutions of the continuous and discrete schemes (2.6) and (2.23), respectively. In addition, let $\widehat{\boldsymbol{\sigma}}_h$ and $(p_h,\mathbf{u}_h)$ be the discrete approximations introduced in (2.24) and (2.26), respectively. Assume that for some $s\in[1,k+1]$ there hold $\mathbf{t}\big|_K$, $\boldsymbol{\sigma}\big|_K\in\mathbb{H}^s(K)$, $\mathbf{div}(\boldsymbol{\sigma})\big|_K\in\mathbf{H}^s(K)$, and $\mathbf{u}\big|_K\in\mathbf{H}^s(K)$ for each $K\in\mathcal{T}_h$. Then, there exist positive constants C_1 and C_2, independent of h, such that

$$\|\boldsymbol{\sigma}-\widehat{\boldsymbol{\sigma}}_h\|_{0,\Omega} + \|p-p_h\|_{0,\Omega} \;\le\; C_1\,h^s \sum_{K\in\mathcal{T}_h}\Big\{|\mathbf{t}|_{s,K} + |\boldsymbol{\sigma}|_{s,K} + |\mathbf{div}(\boldsymbol{\sigma})|_{s,K}\Big\}\,, \tag{2.27}$$

and

$$\|\mathbf{u}-\mathbf{u}_h\|_{0,\Omega} \;\le\; C_2\,h^s \sum_{K\in\mathcal{T}_h}\Big\{|\mathbf{u}|_{s,K} + |\mathbf{t}|_{s,K} + |\boldsymbol{\sigma}|_{s,K} + |\mathbf{div}(\boldsymbol{\sigma})|_{s,K}\Big\}\,. \tag{2.28}$$

Proof. See [23, Theorem 4.3]. $\square$

Theorem 2.5. Assume that the hypotheses of Theorem 2.4 are satisfied. Then, there exists a positive constant C, independent of h, such that

$$\Big\{\sum_{K\in\mathcal{T}_h}\|\boldsymbol{\sigma}-\boldsymbol{\sigma}_{h,K}^{\star}\|_{\mathbf{div};K}^2\Big\}^{1/2} \;\le\; C\,h^s \sum_{K\in\mathcal{T}_h}\Big\{|\mathbf{t}|_{s,K} + |\boldsymbol{\sigma}|_{s,K} + |\mathbf{div}(\boldsymbol{\sigma})|_{s,K}\Big\}\,. \tag{2.29}$$

Proof. See [23, Theorem 4.4]. $\square$

Finally, we recall here that the approximation $\boldsymbol{\sigma}_{h,K}^{\star}$ is introduced to improve the non-satisfactory order provided by the first approximation $\widehat{\boldsymbol{\sigma}}_{h,K}$ with respect to the broken $\mathbb{H}(\mathbf{div})$-norm. This fact was substantiated numerically in [23, Section 5].

3 A posteriori error analysis

In this section we present details about an a posteriori error analysis for the mixed virtual element scheme (2.23). For this purpose, we follow the approach from [17], which allows us to establish an adaptive strategy bearing in mind the two approximations of $\boldsymbol{\sigma}_h$ introduced in Section 2.2.2.

We start by introducing some useful notation. Let $\mathcal{E}_h$ be the set of all edges of $\mathcal{T}_h$, and $\mathcal{E}(K)$ denotes the set of edges of a given $K\in\mathcal{T}_h$. Then $\mathcal{E}_h=\mathcal{E}_h(\Omega)\cup\mathcal{E}_h(\Gamma)$, where $\mathcal{E}_h(\Omega):=\{e\in\mathcal{E}_h:\quad e\subseteq\Omega\}$ and

$\mathcal{E}_h(\Gamma) := \{e \in \mathcal{E}_h : \quad e \subseteq \Gamma\}$. Moreover, h_e stands for the length of a given edge e. Also, for each edge $e \in \mathcal{E}_h$ we fix a unit normal vector $\boldsymbol{\nu}_e := (\nu_1, \nu_2)^{\mathbf{t}}$, and let $\boldsymbol{s}_e := (-\nu_2, \nu_1)^{\mathbf{t}}$ be the corresponding fixed unit tangential vector along e. However, when no confusion arises, we simply write $\boldsymbol{\nu}$ and $\boldsymbol{s}$ instead of $\boldsymbol{\nu}_e$ and $\boldsymbol{s}_e$, respectively. Now, given $\boldsymbol{\zeta} \in \mathbb{L}^2(\Omega)$ such that $\boldsymbol{\zeta}\big|_K \in \mathbb{C}(K)$ for each $K \in \mathcal{T}_h$ and $e \in \mathcal{E}_h(\Omega)$, we denote by $[\![\boldsymbol{\zeta s}]\!]$ the tangential jump of $\boldsymbol{\zeta}$ across e, that is $[\![\boldsymbol{\zeta s}]\!] := (\boldsymbol{\zeta}\big|_K - \boldsymbol{\zeta}\big|_{K'})\big|_e \boldsymbol{s}$, where K and K' are the elements of $\mathcal{T}_h$ having e as a common edge. Finally, given scalar, vector and tensor valued fields $v, \boldsymbol{\varphi} := (\varphi_1, \varphi_2)^{\mathbf{t}}$ and $\boldsymbol{\tau} := (\tau_{ij})$, respectively, we let

$$\mathbf{curl}(v) := \begin{pmatrix} \frac{\partial v}{\partial x_2} \\ -\frac{\partial v}{\partial x_1} \end{pmatrix}^{\mathbf{t}}, \qquad \underline{\mathbf{curl}}(\boldsymbol{\varphi}) := \begin{pmatrix} \mathbf{curl}(\varphi_1)^{\mathbf{t}} \\ \mathbf{curl}(\varphi_2)^{\mathbf{t}} \end{pmatrix} \qquad \text{and} \qquad \mathrm{curl}(\boldsymbol{\tau}) := \begin{pmatrix} \frac{\partial \tau_{12}}{\partial x_1} - \frac{\partial \tau_{11}}{\partial x_2} \\ \frac{\partial \tau_{22}}{\partial x_1} - \frac{\partial \tau_{21}}{\partial x_2} \end{pmatrix}.$$

In what follows we assume the hypotheses of Theorems 2.1 and 2.2 and let $(\mathbf{t}, \boldsymbol{\sigma}) \in X \times H$ and $(\mathbf{t}_h, \boldsymbol{\sigma}_h) \in X_k^h \times H_k^h$ be the unique solutions of (2.6) and (2.23), respectively. In addition, let $\widehat{\boldsymbol{\sigma}}_{h,K}$, $\boldsymbol{\sigma}^\star_{h,K}$ and $\mathbf{u}_h$ be the approximations introduced in Section 2.2.2. Then, we define for each $K \in \mathcal{T}_h$ the local a posteriori error indicators

$$\Psi_K^2 := \Lambda_{1,K}^2 + \Lambda_{2,K}^2 + \Lambda_{3,K}^2 + \|\boldsymbol{\sigma}^{\star,\mathbf{d}}_{h,K} - \mu(|\mathbf{t}_h|)\mathbf{t}_h\|_{0,K}^2 ,$$

and

$$\theta_K^2 := \Lambda_{4,K}^2 + h_K^2\|\mathbf{t}_h - \nabla \mathbf{u}_h\|_{0,K}^2 + h_K^2 \|\mathrm{curl}(\mathbf{t}_h)\|_{0,K}^2 + \sum_{e \in \mathcal{E}(K) \cap \mathcal{E}_h(\Omega)} h_e \|[\![\mathbf{t}_h \boldsymbol{s}]\!]\|_{0,e}^2$$
$$+ \sum_{e \in \mathcal{E}(K) \cap \mathcal{E}_h(\Gamma)} h_e \left\{ \|\mathbf{g} - \mathbf{u}_h\|_{0,e}^2 + \left\| \frac{d\mathbf{g}}{d\boldsymbol{s}} - \mathbf{t}_h \boldsymbol{s} \right\|_{0,e}^2 \right\} ,$$

where $\boldsymbol{\sigma}^{\star,\mathbf{d}}_{h,K}$ is denoting the deviator tensor of $\boldsymbol{\sigma}^\star_{h,K}$, and

$$\begin{aligned} \Lambda_{1,K}^2 &:= \mathcal{S}^K(\boldsymbol{\sigma}_h - \widehat{\boldsymbol{\sigma}}_{h,K}, \boldsymbol{\sigma}_h - \widehat{\boldsymbol{\sigma}}_{h,K}) , \qquad & \Lambda_{2,K}^2 &:= \|\boldsymbol{\sigma}^\star_{h,K} - \widehat{\boldsymbol{\sigma}}_{h,K}\|_{0,K}^2 , \\ \Lambda_{3,K}^2 &:= \|\mathbf{div}(\boldsymbol{\sigma}_h - \boldsymbol{\sigma}^\star_{h,K})\|_{0,K}^2 , & \Lambda_{4,K}^2 &:= \frac{1}{\alpha^2}\|\mathbf{f} - \mathcal{P}_k^K(\mathbf{f})\|_{0,K}^2 . \end{aligned} \tag{3.1}$$

We observe that the term $\frac{d\mathbf{g}}{d\boldsymbol{s}}$ in θ_K^2 requires the trace $\mathbf{g}$ to be more regular, in particular, we need that $\mathbf{g} \in \mathbf{H}^1(\Gamma)$. Then, we introduce the global error estimator given by

$$\boldsymbol{\eta} := \left\{ \sum_{K \in \mathcal{T}_h} \left\{ \Psi_K^2 + \theta_K^2 \right\} \right\}^{1/2} . \tag{3.2}$$

The following theorem constitutes the main result of this section

Theorem 3.1. Let $(\mathbf{t}, \boldsymbol{\sigma}) \in X \times H$ and $(\mathbf{t}_h, \boldsymbol{\sigma}_h) \in X_k^h \times H_k^h$ be the unique solutions of the problem (2.6) and (2.23), respectively. In addition, let $\boldsymbol{\sigma}^\star_{h,K}$ be the discrete approximation introduced in (2.25). Furthermore, assume that the data $\mathbf{g} \in \mathbf{H}^1(\Gamma)$ and $\dfrac{d\mathbf{g}}{d\boldsymbol{s}}$ is piecewise polynomial. Then, there exist positives constants $C_{\mathtt{eff}}$ and $C_{\mathtt{rel}}$, independent of h, such that

$$\|\mathbf{u} - \mathbf{u}_h\|_{0,\Omega} + \|(\mathbf{t}, \boldsymbol{\sigma}) - (\mathbf{t}_h, \boldsymbol{\sigma}_h)\|_{X \times H} + \left\{ \sum_{K \in \mathcal{T}_h} \|\boldsymbol{\sigma} - \boldsymbol{\sigma}^\star_{h,K}\|_{\mathbf{div};K}^2 \right\}^{1/2} \leq C_{\mathtt{rel}} \boldsymbol{\eta} , \tag{3.3}$$

and

$$C_{\mathtt{eff}} \boldsymbol{\eta} \leq \|\mathbf{u} - \mathbf{u}_h\|_{0,\Omega} + \|(\mathbf{t}, \boldsymbol{\sigma}) - (\mathbf{t}_h, \boldsymbol{\sigma}_h)\|_{X \times H} + \left\{ \sum_{K \in \mathcal{T}_h} \|\boldsymbol{\sigma} - \boldsymbol{\sigma}^\star_{h,K}\|_{\mathbf{div};K}^2 \right\}^{1/2} + \|\boldsymbol{\sigma} - \boldsymbol{\mathcal{P}}_k^h(\boldsymbol{\sigma})\|_{0,\Omega} . \tag{3.4}$$

The proof of the Theorem 3.1 is separated into the two parts given by the next subsections. More precisely, we show lower and upper bounds for the error that involves the discrete approximations $\boldsymbol{\sigma}^{\star}_{h,K}$, which were introduced in Section 2.2.2, and the global error estimator defined in (3.2). In Section 3.1 we prove that $\boldsymbol{\eta}$ satisfy reliability properties, whereas the corresponding efficiency properties are derived in Section 3.2.

3.1 Reliability

We proceed with the following preliminary estimate.

Lemma 3.1. Let $(\mathbf{t},\boldsymbol{\sigma}) \in X \times H$ and $(\mathbf{t}_h,\boldsymbol{\sigma}_h) \times X^h_k \times H^h_k$ be the unique solutions of (2.6) and (2.23), respectively. Then, there exists a positive constant C, such that

$$C\|(\mathbf{t},\boldsymbol{\sigma}) - (\mathbf{t}_h,\boldsymbol{\sigma}_h)\|_{X\times H} \;\le\; \left\{ \sum_{K\in\mathcal{T}_h} \left\{ \Lambda^2_{1,K} + \Lambda^2_{2,K} + \|\boldsymbol{\sigma}^{\star,\mathbf{d}}_{h,K} - \mu(|\mathbf{t}_h|)\mathbf{t}_h\|^2_{0,K} \right\} \right\}^{1/2} + \sup_{\substack{\boldsymbol{\tau}\in H\\ \boldsymbol{\tau}\neq\mathbf{0}}} \frac{\mathcal{R}(\boldsymbol{\tau})}{\|\boldsymbol{\tau}\|_H}\,, \tag{3.5}$$

where

$$\mathcal{R}(\boldsymbol{\tau}) \;:=\; -\int_\Omega \mathbf{t}_h : (\boldsymbol{\tau} - \boldsymbol{\tau}_h) + \langle(\boldsymbol{\tau} - \boldsymbol{\tau}_h)\boldsymbol{\nu},\mathbf{g}\rangle \;-\; \frac{1}{\alpha}\int_\Omega (\mathbf{f} + \mathbf{div}(\boldsymbol{\sigma}_h)) \cdot \mathbf{div}(\boldsymbol{\tau} - \boldsymbol{\tau}_h) \tag{3.6}$$

for all $(\mathbf{s},\boldsymbol{\tau}_h) \in X^h_k \times H^h_k$ such that $\|(\mathbf{s}_h,\boldsymbol{\tau}_h)\|_{X\times H} \le C\|(\mathbf{s},\boldsymbol{\tau})\|_{X\times H}$ for some positive constant C independent of $(\mathbf{s},\boldsymbol{\tau})$.

Proof. Proceeding as in [20, Section 5.2], together with the fact that the nonlinear operator $\mathbb{A}$ (cf. (2.2)), has Gâteaux derivative $\mathcal{D}\mathbb{A}(\widetilde{\mathbf{r}})$ at any $\widetilde{\mathbf{r}} \in X$, it is possible to deduce that the linear operator $\mathcal{M} : X \times H \to (X \times H)'$ defined by

$$[\mathcal{M}(\mathbf{s},\boldsymbol{\tau}),(\mathbf{r},\boldsymbol{\zeta})] \;:=\; \mathcal{D}\mathbb{A}(\widetilde{\mathbf{r}})(\mathbf{r},\mathbf{s}-\kappa\boldsymbol{\tau}^{\mathbf{d}}) - \int_\Omega \mathbf{s} : \boldsymbol{\zeta}^{\mathbf{d}} + \int_\Omega \mathbf{r} : \boldsymbol{\tau}^{\mathbf{d}} + \kappa\int_\Omega \boldsymbol{\zeta}^{\mathbf{d}} : \boldsymbol{\tau}^{\mathbf{d}} + \frac{1}{\alpha}\int_\Omega \mathbf{div}(\boldsymbol{\zeta})\cdot\mathbf{div}(\boldsymbol{\tau})$$

for all $(\mathbf{s},\boldsymbol{\tau}),(\mathbf{r},\boldsymbol{\zeta}) \in X \times H$, satisfies a global inf-sup condition. More precisely, there exists a constant $C > 0$, independent of h, such that

$$C\|(\mathbf{r},\boldsymbol{\zeta})\|_{X\times H} \;\le\; \sup_{\substack{(\mathbf{s},\boldsymbol{\tau})\in X\times H\\ (\mathbf{s},\boldsymbol{\tau})\neq\mathbf{0}}} \frac{[\mathcal{M}(\mathbf{s},\boldsymbol{\tau}),(\mathbf{r},\boldsymbol{\zeta})]}{\|(\mathbf{s},\boldsymbol{\tau})\|_{X\times H}}\,. \tag{3.7}$$

for all $\widetilde{\mathbf{r}} \in X$ and for all $(\mathbf{r},\boldsymbol{\zeta}) \in X \times H$. Next, since $\mathbf{t},\mathbf{t}_h \in X$, the mean value theorem ensure the existence of $\widetilde{\mathbf{r}}_h \in X$, such that

$$\mathcal{D}\mathbb{A}(\widetilde{\mathbf{r}}_h)(\mathbf{t}-\mathbf{t}_h,\mathbf{s}) \;=\; [\mathbb{A}(\mathbf{t}) - \mathbb{A}(\mathbf{t}_h),\mathbf{s}] \qquad \forall\,\mathbf{s}\in X\,.$$

Then, applying (3.7) to the error $(\mathbf{r},\boldsymbol{\zeta}) := (\mathbf{t}-\mathbf{t}_h,\boldsymbol{\sigma}-\boldsymbol{\sigma}_h)$, we get

$$C\|(\mathbf{t},\boldsymbol{\sigma}) - (\mathbf{t}_h,\boldsymbol{\sigma}_h)\|_{X\times H} \;\le\; \sup_{\substack{(\mathbf{s},\boldsymbol{\tau})\in X\times H\\ (\mathbf{s},\boldsymbol{\tau})\neq\mathbf{0}}} \frac{[\mathbf{A}(\mathbf{t},\boldsymbol{\sigma}) - \mathbf{A}(\mathbf{t}_h,\boldsymbol{\sigma}_h),(\mathbf{s},\boldsymbol{\tau})]}{\|(\mathbf{s},\boldsymbol{\tau})\|_{X\times H}}\,. \tag{3.8}$$

Furthermore, from (2.6), (2.23), and adding and subtracting suitable terms, we realize that

$$\begin{aligned}
[\mathbf{A}(\mathbf{t},\boldsymbol{\sigma}) - \mathbf{A}(\mathbf{t}_h,\boldsymbol{\sigma}_h),(\mathbf{s},\boldsymbol{\tau})] \;&=\; [\mathbf{F},(\mathbf{s},\boldsymbol{\tau})] - [\mathbf{A}(\mathbf{t}_h,\boldsymbol{\sigma}_h),(\mathbf{s},\boldsymbol{\tau})]\\
&=\; [\mathbf{F},(\mathbf{s}-\mathbf{s}_h,\boldsymbol{\tau}-\boldsymbol{\tau}_h)] + [\mathbf{F},(\mathbf{s}_h,\boldsymbol{\tau}_h)] - [\mathbf{A}(\mathbf{t}_h,\boldsymbol{\sigma}_h),(\mathbf{s},\boldsymbol{\tau})]\\
&=\; [\mathbf{F},(\mathbf{s}-\mathbf{s}_h,\boldsymbol{\tau}-\boldsymbol{\tau}_h)] + [\mathbf{A}_h(\mathbf{t}_h,\boldsymbol{\sigma}_h),(\mathbf{s}_h,\boldsymbol{\tau}_h)]\\
&\quad\; - [\mathbf{A}(\mathbf{t}_h,\boldsymbol{\sigma}_h),(\mathbf{s},\boldsymbol{\tau})]\\
&=\; [\mathbf{F},(\mathbf{s}-\mathbf{s}_h,\boldsymbol{\tau}-\boldsymbol{\tau}_h)] + [\mathbf{A}_h(\mathbf{t}_h,\boldsymbol{\sigma}_h) - \mathbf{A}(\mathbf{t}_h,\boldsymbol{\sigma}_h),(\mathbf{s}_h,\boldsymbol{\tau}_h)]\\
&\quad\; - [\mathbf{A}(\mathbf{t}_h,\boldsymbol{\sigma}_h),(\mathbf{s}-\mathbf{s}_h,\boldsymbol{\tau}-\boldsymbol{\tau}_h)]
\end{aligned} \tag{3.9}$$

for a given $(\mathbf{s},\boldsymbol{\tau}) \in X \times H$ and any $(\mathbf{s}_h,\boldsymbol{\tau}_h) \in X_k^h \times H_k^h$

Now, in what follows we assume that $(\mathbf{s}_h,\boldsymbol{\tau}_h) \in X_k^h \times H_k^h$ is chosen such that $\|(\mathbf{s}_h,\boldsymbol{\tau}_h)\|_{X\times H} \leq C\|(\mathbf{s},\boldsymbol{\tau})\|_{X\times H}$ for some positive constant C independent of $(\mathbf{s},\boldsymbol{\tau})$. Hence, from Lemma 2.1, the inequality (2.21), and the expresions in (3.1), we deduce

$$[\mathbf{A}_h(\mathbf{t}_h,\boldsymbol{\sigma}_h)-\mathbf{A}(\mathbf{t}_h,\boldsymbol{\sigma}_h),(\mathbf{s}_h,\boldsymbol{\tau}_h)] \;\leq\; C\Big\{\sum_{K\in\mathcal{T}_h}\Big\{\Lambda_{1,K}^2+\Lambda_{2,K}^2+\|\boldsymbol{\sigma}_{h,K}^{\star,\mathbf{d}}-\mu(|\mathbf{t}_h|)\mathbf{t}_h\|_{0,K}^2\Big\}\Big\}^{1/2}\|(\mathbf{s},\boldsymbol{\tau})\|_{X\times H}\,, \tag{3.10}$$

with a constant $C>0$, independent of h. On the other hand, from (2.7) and (2.8), adding and subtracting suitable terms, and then performing some algebraic manipulations, we find that

$$\begin{aligned}
&[\mathbf{F},(\mathbf{s}-\mathbf{s}_h,\boldsymbol{\tau}-\boldsymbol{\tau}_h)]-[\mathbf{A}(\mathbf{t}_h,\boldsymbol{\sigma}_h),(\mathbf{s}-\mathbf{s}_h,\boldsymbol{\tau}-\boldsymbol{\tau}_h)]\\
&\qquad = \int_\Omega \big\{\widehat{\boldsymbol{\sigma}}_h^{\mathbf{d}}-\mu(|\mathbf{t}_h|)\mathbf{t}_h\big\}:\big\{(\mathbf{s}-\mathbf{s}_h)-\kappa(\boldsymbol{\tau}-\boldsymbol{\tau}_h)^{\mathbf{d}}\big\}\\
&\qquad\quad + \int_\Omega(\boldsymbol{\sigma}_h-\widehat{\boldsymbol{\sigma}}_h):\big\{(\mathbf{s}-\mathbf{s}_h)-\kappa(\boldsymbol{\tau}-\boldsymbol{\tau}_h)^{\mathbf{d}}\big\}+\mathcal{R}(\boldsymbol{\tau})\,,
\end{aligned} \tag{3.11}$$

where $\mathcal{R}(\boldsymbol{\tau})$ is given by (3.6). Then, from (3.8)–(3.11), using the Cauchy-Schwarz inequality, adding and subtracting locally $\boldsymbol{\sigma}_{h,K}^{\star,\mathbf{d}}$, and recalling that $\|(\mathbf{s}_h,\boldsymbol{\tau}_h)\|_{X\times H} \leq C\|(\mathbf{s},\boldsymbol{\tau})\|_{X\times H}$, we conclude the proof. $\square$

We now aim to bound the supremum on the right-hand side of (3.5). In order to do that, we need a suitable choice of $(\mathbf{s}_h,\boldsymbol{\tau}_h) \in X_k^h \times H_k^h$. To this end, given $(\mathbf{s},\boldsymbol{\tau}) \in X \times H$, we take by simplicity $\mathbf{s}_h := \boldsymbol{\mathcal{P}}_k^h(\mathbf{s}) \in X_k^h$, whereas the choice of $\boldsymbol{\tau}_h$ requires the use of a Clément-type interpolant and the Helmholtz decomposition in H.

Then, proceeding as in [17, Section 5], we make use of the interpolation operator $\mathcal{I}_k^h : \mathbf{H}^1(\Omega) \to V_k^h$, where V_k^h (cf. [3]) is defined for all $k \geq 0$ as

$$V_k^h \;:=\; \Big\{\mathbf{v}\in\mathbf{H}^1(\Omega):\quad \mathbf{v}\big|_{\partial K}\in\mathbb{B}_k(\partial K)\quad\text{and}\quad \Delta\mathbf{v}\in\mathbf{P}_{k-1}(K)\quad\forall K\in\mathcal{T}_h\Big\}\,,$$

with

$$\mathbb{B}_k(\partial K) \;:=\; \Big\{\mathbf{v}\in\mathbf{C}(\partial K):\quad \mathbf{v}|_e\in\mathbf{P}_{k+1}(e)\quad\forall\text{ edge } e\subseteq\partial K\Big\}\,.$$

Next, the following lemma establishes the local approximation properties of $\mathcal{I}_h$.

Lemma 3.2. There exist constants $c_1, c_2 > 0$, independent of h, such that for all $\mathbf{v} \in \mathbf{H}^1(\Omega)$ there hold

$$\|\mathbf{v}-\mathcal{I}_k^h(\mathbf{v})\|_{0,K} \;\leq\; c_1 h_K\|\mathbf{v}\|_{1,\omega_K}\qquad\forall\, K\in\mathcal{T}_h\,, \tag{3.12}$$

and

$$\|(\mathbf{v}-\mathcal{I}_k^h(\mathbf{v}))\cdot\boldsymbol{\nu}_e\|_{0,e} \;\leq\; c_2 h_e^{1/2}\|\mathbf{v}\|_{1,\omega_e}\qquad\forall\, e\in\mathcal{E}_h\,, \tag{3.13}$$

where $\omega_K := \{K' \in \mathcal{T}_h :\;\; K \cap K' \neq \varnothing\}$ and $\omega_e := \{K \in \mathcal{T}_h :\;\; e \in \mathcal{E}(K)\}$.

Proof. See [29, Section 4, Proposition 4.2] and [17, Section 5, eq. 24] for more details. $\square$

Now, for each $\boldsymbol{\tau} \in H$ we consider its Helmholtz decomposition (see, e.g, [21, Section 4])

$$\boldsymbol{\tau} \;=\; \nabla\mathbf{z} + \underline{\mathbf{curl}}\,(\boldsymbol{\varphi})\,, \tag{3.14}$$

where $\mathbf{z} \in \mathbf{H}^2(\Omega)$ and $\boldsymbol{\varphi} \in \mathbf{H}^1(\Omega)$, are such that $\mathbf{div}\,(\nabla\mathbf{z}) = \mathbf{div}\,(\boldsymbol{\tau})$ in Ω, and there holds

$$\|\mathbf{z}\|_{2,\Omega} + \|\boldsymbol{\varphi}\|_{1,\Omega} \;\leq\; C\|\boldsymbol{\tau}\|_{\mathbf{div};\Omega}\,, \tag{3.15}$$

with C a positive constant independent of all the foregoing variables. Then, recalling that $\mathcal{I}_k^h : \mathbf{H}^1(\Omega) \to V_k^h$ and $\mathbf{\Pi}_k^h : \mathbb{H}^1(\Omega) \to H_k^h$ are the respective interpolation operators on V_k^h and H_k^h, letting $\boldsymbol{\zeta} := \nabla \mathbf{z} \in \mathbb{H}^1(\Omega)$, $\boldsymbol{\varphi}_h := \mathcal{I}_k^h(\boldsymbol{\varphi})$, and using Lemma 5.1 in [17, Section 5], we set

$$\boldsymbol{\tau}_h \;:=\; \mathbf{\Pi}_k^h(\boldsymbol{\zeta}) \,+\, \underline{\mathbf{curl}}\,(\boldsymbol{\varphi}_h) \,+\, c_h \mathbb{I}\,, \tag{3.16}$$

where $c_h \in \mathrm{R}$ is chosen so that $\boldsymbol{\tau}_h \in H_k^h$. Equivalently, $\boldsymbol{\tau}_h$ is the $\mathbb{H}_0(\mathbf{div};\Omega)$-component of $\underline{\mathbf{curl}}(\boldsymbol{\varphi}_h) + \Pi_k^h(\boldsymbol{\zeta})$. In addition, it follows from our chosen for $(\mathbf{s}_h, \boldsymbol{\tau}_h)$, by applying of the triangle inequality, the estimates (2.16), (3.12), and the property (3.15), that there holds $\|(\mathbf{s}_h, \boldsymbol{\tau}_h)\|_{X\times H} \le C\|(\mathbf{s}, \boldsymbol{\tau})\|_{X\times H}$ for some $C > 0$ independent of $(\mathbf{s}, \boldsymbol{\tau})$.

Now, according to (3.14), (3.16), and the linearity of $\mathcal{R}$ (cf. (3.6)), we deduce that the expression $\mathcal{R}(\boldsymbol{\tau})$ can be rewritten as

$$\mathcal{R}(\boldsymbol{\tau}) \;=\; \mathcal{R}(\boldsymbol{\zeta} - \mathbf{\Pi}_k^h(\boldsymbol{\zeta})) \,+\, \mathcal{R}(\underline{\mathbf{curl}}(\boldsymbol{\varphi} - \boldsymbol{\varphi}_h)) \,+\, c_h \mathcal{R}_{\mathbb{I}}\,,$$

where

$$\mathcal{R}_{\mathbb{I}} \;:=\; \int_\Omega \mathbf{t}_h : \mathbb{I}^{\mathbf{d}} \,-\, \langle \mathbb{I}\boldsymbol{\nu}, \mathbf{g}\rangle \,+\, \frac{1}{\alpha}\int_\Omega (\mathbf{f} + \mathbf{div}(\boldsymbol{\sigma}_h)) \cdot \mathbf{div}(\mathbb{I})\,.$$

Then, using that $\mathbb{I}^{\mathbf{d}} = \mathbf{0}$, $\mathbf{div}(\mathbb{I}) = \mathbf{0}$ and the fact that $\langle \mathbb{I}\boldsymbol{\nu}, \mathbf{g}\rangle = 0$ (which is a consequence of the compatibility condition for the Dirichlet datum $\mathbf{g}$ explained in Section 2.1), we obtain

$$\mathcal{R}(\boldsymbol{\tau}) \;=\; \mathcal{R}(\boldsymbol{\zeta} - \mathbf{\Pi}_k^h(\boldsymbol{\zeta})) \,+\, \mathcal{R}(\underline{\mathbf{curl}}(\boldsymbol{\varphi} - \boldsymbol{\varphi}_h))\,. \tag{3.17}$$

Next, the following lemma yields the required bound for the supremum on the right-hand side of (3.5).

Lemma 3.3. Assume that $\mathbf{g} \in \mathbf{H}^1(\Gamma)$. Then, there exists $C > 0$, independent of h, such that

$$|\mathcal{R}(\boldsymbol{\tau})| \;\le\; C\left\{\sum_{K\in\mathcal{T}_h} \theta_K^2\right\}^{1/2} \|\boldsymbol{\tau}\|_H\,.$$

Proof. It is follows after to bound the modules of the two expressions on the right-hand side of (3.17). To bound $|\mathcal{R}(\boldsymbol{\zeta} - \mathbf{\Pi}_k^h(\boldsymbol{\zeta}))|$, we use the ideas from Lemma 5.8 in [17, Section 5], together to the identity

$$\mathbf{div}(\boldsymbol{\zeta} - \mathbf{\Pi}_k^h(\boldsymbol{\zeta})) \;=\; (\mathbf{I} - \mathcal{P}_k^h)(\mathbf{div}(\boldsymbol{\tau}))\,,$$

which is consequence of (2.17), and the fact that $\mathbf{div}(\boldsymbol{\zeta}) = \mathbf{div}(\boldsymbol{\tau})$ in Ω, and where $\mathbf{I}$ is denoting a generic identity operator. In addition, following similar arguments to the proof of Lemma 5.4 in [20, Section 5] (see also [17, Lemma 5.9]), in join with Lemma 3.2, and the fact that the number of elements in ω_e is bounded, the term $|\mathcal{R}(\underline{\mathbf{curl}}(\boldsymbol{\varphi} - \boldsymbol{\varphi}_h))|$ is suitably bounded. $\square$

Then, as a consequence of Lemmas 3.1 and 3.3, the triangle inequality, and the lower bound in (2.21), we conclude that there exists $C > 0$, independent of h, such that

$$\begin{aligned}
\|(\mathbf{t}, \boldsymbol{\sigma}) - (\mathbf{t}_h, \boldsymbol{\sigma}_h)\|_{X\times H} \,&+\, \left\{\sum_{K\in\mathcal{T}_h} \|\boldsymbol{\sigma} - \boldsymbol{\sigma}_{h,K}^\star\|_{\mathbf{div};K}^2\right\}^{1/2} \\
&\le\; C\left\{\|(\mathbf{t}, \boldsymbol{\sigma}) - (\mathbf{t}_h, \boldsymbol{\sigma}_h)\|_{X\times H} \,+\, \left\{\sum_{K\in\mathcal{T}_h}\left\{\Lambda_{1,K}^2 + \Lambda_{2,K}^2 + \Lambda_{3,K}^2\right\}\right\}^{1/2}\right\} \\
&\le\; C\,\boldsymbol{\eta}
\end{aligned} \tag{3.18}$$

where $\boldsymbol{\eta}$ is the global estimator defined by (3.2). Now, in order to incorporate the error $\|\mathbf{u}-\mathbf{u}_h\|_{0,\Omega}$, we recall that from (2.1) and (2.26), we have that

$$\mathbf{u} \;=\; \frac{1}{\alpha}\Big\{\mathbf{f}+\mathbf{div}\,(\boldsymbol{\sigma})\Big\} \qquad \text{and} \qquad \mathbf{u}_h \;=\; \frac{1}{\alpha}\Big\{\mathcal{P}_k^h(\mathbf{f})+\mathbf{div}\,(\boldsymbol{\sigma}_h)\Big\}\,, \tag{3.19}$$

whence,

$$\|\mathbf{u}-\mathbf{u}_h\|_{0,\Omega} \;\leq\; \frac{1}{\alpha}\Big\{\|\mathbf{f}-\mathcal{P}_k^h(\mathbf{f})\|_{0,\Omega}+\|\boldsymbol{\sigma}-\boldsymbol{\sigma}_h\|_H\Big\}\,. \tag{3.20}$$

Finally, from (3.18) and (3.20) we have that there exists $C_{\mathtt{rel}}>0$, independent of h, such that

$$\|\mathbf{u}-\mathbf{u}_h\|_{0,\Omega} \;+\; \|(\mathbf{t},\boldsymbol{\sigma})-(\mathbf{t}_h,\boldsymbol{\sigma}_h)\|_{X\times H} \;+\; \left\{\sum_{K\in\mathcal{T}_h}\|\boldsymbol{\sigma}-\boldsymbol{\sigma}^\star_{h,K}\|^2_{\mathbf{div};K}\right\}^{1/2} \;\leq\; C_{\mathtt{rel}}\boldsymbol{\eta}\,,$$

which proves the reliability of the estimator $\boldsymbol{\eta}$.

3.2 Efficiency

In this section we prove the efficiency of our a posteriori error estimator $\boldsymbol{\eta}$ (lower bound in (3.4)). For this purpose, we derive suitable upper bounds for the terms defining the local error indicators. First, using the upper bound in (2.21), the estimate (3.19), and adding and subtracting suitable terms, we get

$$\begin{aligned}
\Lambda^2_{1,K} &\leq 4\,\widehat{c}_1\Big\{\|\boldsymbol{\sigma}-\boldsymbol{\sigma}^\star_{h,K}\|^2_{0,K}+\Lambda^2_{2,K}+\|\boldsymbol{\sigma}-\boldsymbol{\sigma}_h\|^2_{0,K}\Big\}\,,\\
\Lambda^2_{2,K} &\leq 4\Big\{\|\boldsymbol{\sigma}-\boldsymbol{\sigma}^\star_{h,K}\|^2_{0,K}+\|\boldsymbol{\sigma}-\boldsymbol{\sigma}_h\|^2_{0,K}+\|\boldsymbol{\sigma}-\boldsymbol{\mathcal{P}}_k^K(\boldsymbol{\sigma})\|^2_{0,K}\Big\}\,,\\
\Lambda^2_{3,K} &\leq 2\Big\{\|\mathbf{div}(\boldsymbol{\sigma}-\boldsymbol{\sigma}^\star_{h,K})\|^2_{0,K}+\|\mathbf{div}(\boldsymbol{\sigma}-\boldsymbol{\sigma}_h)\|^2_{0,K}\Big\}\,,\\
\Lambda^2_{4,K} &\leq 4\max\{1,\alpha^2\}\Big\{\|\mathbf{u}-\mathbf{u}_h\|^2_{0,K}+\|\mathbf{div}(\boldsymbol{\sigma}-\boldsymbol{\sigma}^\star_{h,K})\|^2_{0,K}+\Lambda^2_{3,K}\Big\}\,.
\end{aligned} \tag{3.21}$$

Moreover, procceding as in [20, Section 5.3, eq. 5.26], that is, adding and subtracting $\boldsymbol{\sigma}^{\mathbf{d}}$, using the second equation in (2.4), the fact that $\|\boldsymbol{\zeta}^{\mathbf{d}}\|_{0,K}\leq\|\boldsymbol{\zeta}\|_{0,K}$ for all $\boldsymbol{\zeta}\in\mathbb{L}^2(K)$, and the Lipschitz-continuity of the operator $\mathbb{A}$ (cf. (2.3)), but restricted to the element $K\in\mathcal{T}_h$ instead of Ω, we deduce that

$$\|\widehat{\boldsymbol{\sigma}}^{\star,\mathbf{d}}_{h,K}-\mu(|\mathbf{t}_h|)\mathbf{t}_h\|^2_{0,K} \;\leq\; 2\Big\{\|\boldsymbol{\sigma}-\boldsymbol{\sigma}^\star_{h,K}\|^2_{0,K} \;+\; \gamma_0^2\,\|\mathbf{t}-\mathbf{t}_h\|^2_{0,K}\Big\}\,. \tag{3.22}$$

Next, the upper bounds of the terms which depend on the mesh parameters h_K and h_e, will be derived below. For this purpose, we make use of the results and estimates proved in [17, Section 5.4], whose proofs use techniques based on bubble functions, extension operators, and discrete trace and inverse inequalities. More precisely, it was used the following Lemma (see [15, 17, 29] for more details).

Lemma 3.4. Given $k\geq 0$ and $K\in\mathcal{T}_h$, there exists a positive constant C_{bub}, independent of h_K, such that

$$C_{\mathrm{bub}}^{-1}\|q\|^2_{0,K} \;\leq\; \|\psi_K^{1/2}q\|^2_{0,K} \;\leq\; C_{\mathrm{bub}}\|q\|^2_{0,K} \qquad \forall\, q\in\mathbf{P}_k(K)\,,$$

and

$$C_{\mathrm{bub}}^{-1}\|q\|_{0,K} \;\leq\; \|\psi_K q\|_{0,K}+h_K|\psi_K q|_{1,K} \;\leq\; C_{\mathrm{bub}}\|q\|_{0,K} \qquad \forall\, q\in\mathbf{P}_k(K)\,.$$

In addition, given $e\in\partial K$, there hold

$$C_{\mathrm{bub}}^{-1}\|q\|^2_{0,e} \;\leq\; \|\psi_e^{1/2}q\|^2_{0,e} \;\leq\; C_{\mathrm{bub}}\|q\|^2_{0,e} \qquad \forall\, q\in\mathbf{P}_k(e)\,,$$

and

$$h_K^{-1/2}\|\psi_e L(q)\|_{0,K} + h_K^{1/2}|\psi_e L(q)|_{1,K} \;\le\; C_{\rm bub}\|q\|_{0,e} \qquad \forall\, q \in \mathbf{P}_k(e)\,,$$

where $K \in \omega_e$ and ω_e is as in Lemma 3.2.

Lemma 3.5. Assume that $\dfrac{d\mathbf{g}}{d\boldsymbol{s}}$ is piecewise polynomial. Then, there exist $C_i > 0$, $i = 1,\dots,4$, independent of h, such that

$$\begin{aligned}
h_K^2\|\mathrm{curl}(\mathbf{t}_h)\|_{0,K}^2 &\le C_1\|\mathbf{t}-\mathbf{t}_h\|_{0,K}^2 \qquad \forall\, K \in \mathcal{T}_h\,,\\
h_e\big\|[\![\mathbf{t}_h\boldsymbol{s}]\!]\big\|_{0,e}^2 &\le C_2\|\mathbf{t}-\mathbf{t}_h\|_{0,\omega_e}^2 \qquad \forall\, e \in \mathcal{E}_h(\Omega)\,,\\
h_K^2\|\mathbf{t}_h - \nabla\mathbf{u}_h\|_{0,K}^2 &\le C_3\Big\{\|\mathbf{u}-\mathbf{u}_h\|_{0,K}^2 + h_K^2\|\mathbf{t}-\mathbf{t}_h\|_{0,K}^2\Big\} \qquad \forall\, K \in \mathcal{T}_h\,,\\
h_e\left\{\|\mathbf{g}-\mathbf{u}_h\|_{0,e}^2 + \left\|\frac{d\mathbf{g}}{d\boldsymbol{s}} - \mathbf{t}_h\boldsymbol{s}\right\|_{0,e}^2\right\} &\le C_4\Big\{\|\mathbf{u}-\mathbf{u}_h\|_{0,\omega_e}^2 + h_{K_e}^2\|\mathbf{t}-\mathbf{t}_h\|_{0,\omega_e}^2\Big\} \qquad \forall\, e \in \mathcal{E}_h(\Gamma)\,,
\end{aligned}$$

where ω_e is as in Lemma 3.2.

Proof. The first two estimates are consequence of [17, Lemma 5.17] through an adaptation of [17, Lemma 5.16]. The third inequality follows from a slight modification of the proof of Lemma 5.14 in [17]. Finally, the last estimate follows the same arguments used in the proof of Lemmas 5.15 and 5.18 of [17]. We remark here that all these proofs makes use of Lemma 3.4. □

Consequently, the efficiency of $\boldsymbol{\eta}$ (lower bound in Lemma 3.1) follows straightforwardly from estimates (3.21)–(3.22), together with Lemma 3.5, after summing up over $K \in \mathcal{T}_h$. We observe here that this bound shows the efficiency of the estimator $\boldsymbol{\eta}$ up to data oscillation. This fact can be interpreted as a quasi-efficiency (see, e.g, [1, 31]).

4 Numerical results

In this section, we present several numerical examples confirming reliability and efficiency of the a posteriori error estimator $\boldsymbol{\eta}$ derived in Section 3, and showing the behavior of the associated adaptive algorithm. We recall here that the condition $\int_\Omega \mathrm{tr}(\boldsymbol{\tau}_h) = 0$ for each $\boldsymbol{\tau}_h \in H_k^h$ was imposed as usual, that is, via a real Lagrange multiplier (see [23, Section 5] for more details). In what follows N stands for the total number of degrees of freedom of (2.23), that is,

$$N \;:=\; 2(k+1)\times\{\text{number of edges } e\in\mathcal{T}_h\} + \frac{(k+2)(7k+3)}{2}\times\{\text{number of elements } K\in\mathcal{T}_h\}+1.$$

Also, the individual errors are defined by

$$\mathsf{e}(\mathbf{u}) \;:=\; \|\mathbf{u}-\mathbf{u}_h\|_{0,\Omega}\,, \qquad \mathsf{e}(\mathbf{t}) \;:=\; \|\mathbf{t}-\mathbf{t}_h\|_{0,\Omega}\,, \qquad \mathsf{e}(p) \;:=\; \|p-p_h\|_{0,\Omega}\,,$$

$$\mathsf{e}(\boldsymbol{\sigma}) \;:=\; \left\{\sum_{K\in\mathcal{T}_h}\|\boldsymbol{\sigma}-\boldsymbol{\sigma}_{h,K}^\star\|_{\mathbf{div};K}^2\right\}^{1/2} \qquad \text{and} \qquad \mathsf{e}(\mathbf{u},\mathbf{t},\boldsymbol{\sigma}) \;:=\; \Big\{[\mathsf{e}(\mathbf{u})]^2 + [\mathsf{e}(\mathbf{t})]^2 + [\mathsf{e}(\boldsymbol{\sigma})]^2\Big\}^{1/2},$$

where $\mathbf{u}_h$ and p_h are computed by the postprocessing formulae (2.26), whereas the effectivity index with respect $\boldsymbol{\eta}$ is given by

$$\mathtt{eff}(\boldsymbol{\eta}) \;:=\; \frac{\mathsf{e}(\mathbf{u},\mathbf{t},\boldsymbol{\sigma})}{\boldsymbol{\eta}}\,.$$

Observe that this quantity is not a true efficiency index, however, it gives information on the behavior of $\boldsymbol{\eta}$. Moreover, in this case, some of the local indicators defined in (3.1) can be interpreted as oscillation terms . At least they must have the same rate of convergence of the global error if the exact solution is smooth enough (see, e.g. [17, Section 5.4]). In Example 1 it is proved numerically

Then, we define the experimental rates of convergence

$$\mathtt{r}(\cdot) \;:=\; -2\,\frac{\log(\mathtt{e}(\cdot)/\mathtt{e}'(\cdot))}{\log(N/N')}\,,$$

where $\mathtt{e}$ and $\mathtt{e}'$ denote the corresponding errors for two consecutive meshes with N and N' the respective degrees of freedom of each decomposition. Similarly, we define:

$$\mathtt{r}(\Lambda_i) \;:=\; -2\,\frac{\log(\Lambda_i/\Lambda_i')}{\log(N/N')}\,,$$

where $\Lambda_i := \left\{ \sum\limits_{K\in\mathcal{T}_h} \Lambda_{i,K}^2 \right\}^{1/2}$. For the tests that include adaptivity, we use for the local a posteriori error indicator $\boldsymbol{\eta}_K := \boldsymbol{\eta}|_K$, the strategy:

(i) Start with a coarse mesh $\mathcal{T}_h$.

(ii) Solve the discrete problem on the current mesh $\mathcal{T}_h$.

(iii) Compute local indicators for each $K \in \mathcal{T}_h$.

(iv) Mark each $K' \in \mathcal{T}_h$ to be refined appyling the rule

$$\boldsymbol{\eta}_{K'} \geq \beta \max_{K\in\mathcal{T}_h} \boldsymbol{\eta}_K,$$

with $\beta \in (0,1)$. Here we use $\beta = 0.35$.

(v) Define the new mesh as actual mesh $\mathcal{T}_h$ and go to step (ii).

Regarding adaptive strategy, for each $K \in \mathcal{T}_h$ that has been marked for refinement, we subdivide it using the midpoint of each edge of the boundary of K and connecting these to its barycenter. Observe that all meshes used for the numerical examples in this section (see Figure 4.1) are composed of convex elements, therefore, the barycenter of K is an internal point of this. In this way, each new element generated with this strategy is a quadrilateral. Now, since for meshes with non-convex elements, it is possible that some barycenter is outside its respective element, we can use the barycenter of $Ker(K)$ to subdivide K.

In turn, the nonlinear algebraic systems are solved by the Newton method with a tolerance of 10^{-6} and taking as initial iteration the solution of the linear Brinkman problem with $\mu = 1$. The numerical results presented below were obtained using a MATLAB code. For all the numerical tests we use $\alpha = 1$ and $\kappa = 0.4$, where the value of κ is chosen according to the Theorems 2.2 and 2.3.

4.1 Example 1

First, we consider the unit square $\Omega := (0,1)^2$, and choose $\mathbf{f}$ and $\mathbf{g}$ such that the exact solution is given by

$$\mathbf{u}(\mathbf{x}) \;:=\; \begin{pmatrix} -\cos(\pi x_1)\sin(\pi x_2) \\ \sin(\pi x_1)\cos(\pi x_2) \end{pmatrix} \qquad \text{and} \qquad p(\mathbf{x}) \;:=\; x_1^2 + x_2^2 - p_0$$

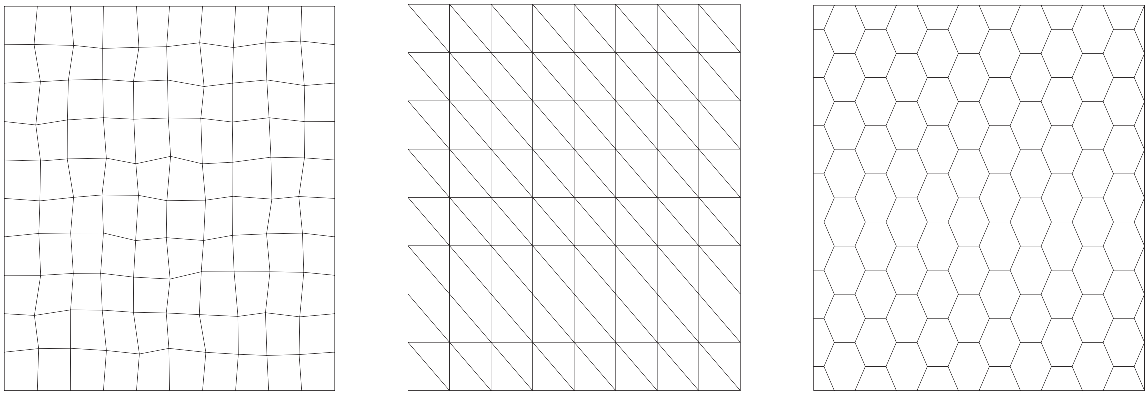

Figure 4.1: Sample meshes: distorted squares (left), triangular (center) and hexagonal (right).

for all $\mathbf{x} := (x_1, x_2)^{\mathbf{t}} \in \Omega$, where $p_0 \in \mathrm{R}$ is such that $\int_\Omega p = 0$. Moreover, we consider the nonlinear viscosity μ given by

$$\mu(s) \;:=\; 2 + (1+s^2)^{-1/6} \qquad \forall\, s \geq 0\,. \tag{4.1}$$

The aim of this test is to verify the asymptotic behavior of the estimator with a smooth solution and under uniform refinements. To this end, we use three families of uniformly generated meshes: distorted squares, uniform triangular and hexagonal (see Figure 4.1).

Tables 4.1 to 4.3 show the convergence history of the errors and the estimator on the three sequence of uniformly refined meshes, indicating that all converge at the optimal rate for polynomial degrees $k = 0, 1, 2$. We can observe the robustness of the estimator with respect to the mesh shape. Moreover, the effectivity of $\boldsymbol{\eta}$ remains bounded. In addition, we see from Table 4.4–4.6 that each term $\Lambda_{i,K}$ for $i = 1, ..., 4$, converge with optimal order $k+1$, with exception of $\Lambda_{3,K}$, which converge with order $k+2$. Also, the robustness of the terms with respect to the mesh shape is verified.

k	N	$\mathtt{e}(\mathbf{u},\mathbf{t},\boldsymbol{\sigma})$	$\mathtt{r}(\mathbf{u},\mathbf{t},\boldsymbol{\sigma})$	$\boldsymbol{\eta}$	$\mathtt{r}(\boldsymbol{\eta})$	$\mathtt{eff}(\boldsymbol{\eta})$
0	741	4.9184e+00	$--$	5.5400e+00	$--$	0.8878
	2881	2.4631e+00	1.0186	2.7848e+00	1.0131	0.8845
	6421	1.6443e+00	1.0084	1.8597e+00	1.0076	0.8842
	11361	1.2342e+00	1.0056	1.3961e+00	1.0050	0.8840
	17701	9.8742e-01	1.0061	1.1173e+00	1.0047	0.8837
1	2381	4.2581e-01	$--$	4.7037e-01	$--$	0.9053
	9361	1.0858e-01	1.9963	1.1968e-01	1.9995	0.9072
	20941	4.8948e-02	1.9790	5.3847e-02	1.9840	0.9090
	37121	2.7384e-02	2.0290	3.0154e-02	2.0256	0.9081
	57901	1.7577e-02	1.9948	1.9348e-02	1.9963	0.9084
2	4721	4.7913e-02	$--$	4.9194e-02	$--$	0.9740
	18641	9.4987e-03	2.3566	9.6137e-03	2.3775	0.9880
	41761	3.0449e-03	2.8209	3.0779e-03	2.8241	0.9893
	74081	1.2901e-03	2.9964	1.3039e-03	2.9968	0.9894
	115601	6.5711e-04	3.0321	6.6436e-04	3.0307	0.9891

Table 4.1: Example 1. Convergence history for a uniformly generated sequence of meshes composed of distorted squares.

k	N	$\mathtt{e}(\mathbf{u},\mathbf{t},\boldsymbol{\sigma})$	$\mathtt{r}(\mathbf{u},\mathbf{t},\boldsymbol{\sigma})$	$\boldsymbol{\eta}$	$\mathtt{r}(\boldsymbol{\eta})$	$\mathtt{eff}(\boldsymbol{\eta})$
0	801	5.0103e+00	−−	5.6443e+00	−−	0.8877
	3137	2.5110e+00	1.0120	2.8399e+00	1.0063	0.8842
	7009	1.6749e+00	1.0074	1.8961e+00	1.0050	0.8834
	12417	1.2565e+00	1.0053	1.4229e+00	1.0039	0.8830
	19361	1.0053e+00	1.0042	1.1387e+00	1.0033	0.8828
1	2753	4.0703e-01	−−	4.7947e-01	−−	0.8489
	10881	1.0774e-01	1.9342	1.2502e-01	1.9561	0.8618
	24385	4.8734e-02	1.9663	5.6304e-02	1.9772	0.8656
	43265	2.7545e-02	1.9902	3.1787e-02	1.9942	0.8666
	67521	1.7659e-02	1.9976	2.0370e-02	1.9994	0.8669
2	5601	4.4640e-02	−−	5.0546e-02	−−	0.8832
	22209	1.0416e-02	2.1128	1.0857e-02	2.2331	0.9594
	49825	3.3845e-03	2.7825	3.5066e-03	2.7973	0.9652
	88449	1.4448e-03	2.9665	1.4962e-03	2.9681	0.9656
	138081	7.4558e-04	2.9705	7.7186e-04	2.9720	0.9660

Table 4.2: Example 1. Convergence history for a uniformly generated sequence of triangular meshes.

k	N	$\mathtt{e}(\mathbf{u},\mathbf{t},\boldsymbol{\sigma})$	$\mathtt{r}(\mathbf{u},\mathbf{t},\boldsymbol{\sigma})$	$\boldsymbol{\eta}$	$\mathtt{r}(\boldsymbol{\eta})$	$\mathtt{eff}(\boldsymbol{\eta})$
0	903	5.1548e+00	−−	5.5410e+00	−−	0.9303
	3891	2.3753e+00	1.0608	2.5969e+00	1.0377	0.9147
	7806	1.6636e+00	1.0230	1.8278e+00	1.0089	0.9102
	13071	1.2797e+00	1.0178	1.4098e+00	1.0074	0.9078
	19686	1.0399e+00	1.0137	1.1474e+00	1.0057	0.9063
1	2723	3.7773e-01	−−	4.2442e-01	−−	0.8810
	11669	8.4064e-02	2.0651	9.3206e-02	2.0835	0.9019
	23414	4.1853e-02	2.0029	4.6318e-02	2.0083	0.9036
	39209	2.4964e-02	2.0045	2.7602e-02	2.0080	0.9044
	59054	1.6562e-02	2.0038	1.8302e-02	2.0065	0.9049
2	5257	5.2896e-02	−−	5.3776e-02	−−	0.9836
	22471	6.9311e-03	2.7980	6.9875e-03	2.8096	0.9919
	45091	2.5194e-03	2.9062	2.5381e-03	2.9082	0.9926
	75511	1.1781e-03	2.9484	1.1865e-03	2.9496	0.9929
	113731	6.4129e-04	2.9700	6.4576e-04	2.9707	0.9931

Table 4.3: Example 1. Convergence history for a uniformly generated sequence of hexagonal meshes.

k	N	Λ_1	$\mathtt{r}(\Lambda_1)$	Λ_2	$\mathtt{r}(\Lambda_2)$	Λ_3	$\mathtt{r}(\Lambda_3)$	Λ_4	$\mathtt{r}(\Lambda_4)$
0	741	1.8477e+00	−−	7.5024e-01	−−	1.5379e-02	−−	4.9244e+00	−−
	2881	9.3401e-01	1.0048	3.7905e-01	1.0056	3.8945e-03	2.0229	2.4657e+00	1.0188
	6421	6.2345e-01	1.0087	2.5285e-01	1.0104	1.7304e-03	2.0244	1.6465e+00	1.0078
	11361	4.6799e-01	1.0053	1.8981e-01	1.0051	9.7493e-04	2.0110	1.2359e+00	1.0054
	17701	3.7456e-01	1.0044	1.5192e-01	1.0043	6.2437e-04	2.0098	9.8875e-01	1.0063
1	2381	1.0284e-01	−−	5.7518e-02	−−	6.9336e-04	−−	4.2232e-01	−−
	9361	2.7016e-02	1.9529	1.4446e-02	2.0185	8.7022e-05	3.0319	1.0808e-01	1.9910
	20941	1.2218e-02	1.9710	6.4404e-03	2.0066	2.5888e-05	3.0115	4.8795e-02	1.9753
	37121	6.9260e-03	1.9831	3.6282e-03	2.0048	1.0944e-05	3.0080	2.7314e-02	2.0270
	57901	4.4529e-03	1.9873	2.3227e-03	2.0065	5.6063e-06	3.0093	1.7539e-02	1.9930
2	4721	4.1684e-03	−−	4.1204e-03	−−	5.5974e-05	−−	4.7853e-02	−−
	18641	6.0907e-04	2.8010	5.1934e-04	3.0162	3.4255e-06	4.0684	9.4926e-03	2.3558
	41761	1.9152e-04	2.8687	1.5552e-04	2.9898	6.7610e-07	4.0235	3.0429e-03	2.8209
	74081	8.3109e-05	2.9129	6.4689e-05	3.0606	2.0539e-07	4.1571	1.2894e-03	2.9959
	115601	4.2959e-05	2.9660	3.3209e-05	2.9969	8.4115e-08	4.0125	6.5675e-04	3.0323

Table 4.4: Example 1. Convergence history of some terms using a uniformly generated sequence of meshes composed of distorted squares.

k	N	Λ_1	$\mathtt{r}(\Lambda_1)$	Λ_2	$\mathtt{r}(\Lambda_2)$	Λ_3	$\mathtt{r}(\Lambda_3)$	Λ_4	$\mathtt{r}(\Lambda_4)$
	801	1.8756e+00	$--$	6.6290e-01	$--$	1.1960e-02	$--$	4.9732e+00	$--$
	3137	9.4552e-01	1.0035	3.3426e-01	1.0031	3.0154e-03	2.0186	2.4931e+00	1.0117
0	7009	6.3131e-01	1.0049	2.2319e-01	1.0048	1.3423e-03	2.0135	1.6631e+00	1.0072
	12417	4.7374e-01	1.0042	1.6749e-01	1.0042	7.5547e-04	2.0103	1.2476e+00	1.0052
	19361	3.7909e-01	1.0036	1.3403e-01	1.0036	4.8362e-04	2.0083	9.9822e-01	1.0042
	2753	1.5275e-01	$--$	5.3977e-02	$--$	6.0926e-04	$--$	4.0644e-01	$--$
	10881	3.8424e-02	2.0084	1.3587e-02	2.0074	7.6697e-05	3.0159	1.0766e-01	1.9332
1	24385	1.7101e-02	2.0064	6.0479e-03	2.0061	2.2760e-05	3.0110	4.8702e-02	1.9661
	43265	9.6244e-03	2.0051	3.4039e-03	2.0049	9.6074e-06	3.0084	2.7527e-02	1.9901
	67521	6.1611e-03	2.0042	2.1791e-03	2.0041	4.9203e-06	3.0068	1.7648e-02	1.9976
	5601	9.6676e-03	$--$	3.3427e-03	$--$	2.9024e-05	$--$	4.4573e-02	$--$
	22209	1.3049e-03	2.9075	4.4608e-04	2.9241	1.9316e-06	3.9342	1.0411e-02	2.1114
2	49825	3.9533e-04	2.9558	1.3486e-04	2.9609	3.8905e-07	3.9663	3.3828e-03	2.7825
	88449	1.6788e-04	2.9847	5.7233e-05	2.9870	1.2382e-07	3.9897	1.4440e-03	2.9665
	138081	8.6179e-05	2.9941	2.9370e-05	2.9957	5.0834e-08	3.9974	7.4520e-04	2.9705

Table 4.5: Example 1. Convergence history of some terms using a uniformly generated sequence of triangular meshes.

k	N	Λ_1	$\mathtt{r}(\Lambda_1)$	Λ_2	$\mathtt{r}(\Lambda_2)$	Λ_3	$\mathtt{r}(\Lambda_3)$	Λ_4	$\mathtt{r}(\Lambda_4)$
	903	1.8103e+00	$--$	7.6139e-01	$--$	1.6158e-02	$--$	5.0494e+00	$--$
	3891	8.8261e-01	0.9836	3.5881e-01	1.0301	3.5023e-03	2.0936	2.3539e+00	1.0450
	7806	6.2697e-01	0.9824	2.5287e-01	1.0052	1.7330e-03	2.0210	1.6545e+00	1.0129
	13071	4.8602e-01	0.9880	1.9519e-01	1.0045	1.0307e-03	2.0161	1.2752e+00	1.0102
	19686	3.9676e-01	0.9911	1.5892e-01	1.0039	6.8250e-04	2.0131	1.0374e+00	1.0078
	2723	1.4070e-01	$--$	6.1339e-02	$--$	7.7155e-04	$--$	3.7815e-01	$--$
	11669	3.0868e-02	2.0848	1.3240e-02	2.1072	7.6419e-05	3.1778	8.4359e-02	2.0619
	23414	1.5308e-02	2.0143	6.5354e-03	2.0276	2.6446e-05	3.0475	4.2013e-02	2.0020
	39209	9.1135e-03	2.0117	3.8807e-03	2.0219	1.2089e-05	3.0367	2.5064e-02	2.0038
	59054	6.0396e-03	2.0091	2.5678e-03	2.0166	6.5029e-06	3.0280	1.6630e-02	2.0033
	5257	5.8995e-03	$--$	3.3259e-03	$--$	3.3573e-05	$--$	5.2785e-02	$--$
	22471	6.2194e-04	3.0975	3.4240e-04	3.1302	1.5341e-06	4.2484	6.9226e-03	2.7969
	45091	2.2035e-04	2.9797	1.1957e-04	3.0212	3.6877e-07	4.0937	2.5165e-03	2.9059
	75511	1.0208e-04	2.9849	5.4821e-05	3.0249	1.2775e-07	4.1120	1.1768e-03	2.9482
	113731	5.5393e-05	2.9850	2.9538e-05	3.0199	5.5315e-08	4.0876	6.4060e-04	2.9699

Table 4.6: Example 1.Convergence history of some terms using a uniformly generated sequence of hexagonal meshes.

4.2 Example 2

We consider again the unit square $\Omega := (0,1)^2$, and choose $\mathbf{f}$ and $\mathbf{g}$ such that the exact solution is given by

$$\mathbf{u}(\mathbf{x}) \; := \; \begin{pmatrix} (1 + x_1 - e^{x_1})(1 - \cos(x_2)) \\ \\ (1 - e^{x_1})(\sin(x_2) - x_2) \end{pmatrix} \qquad \text{and} \qquad p(\mathbf{x}) \; := \; \frac{1}{x_1 + 0.1} - p_0$$

for all $\mathbf{x} := (x_1, x_2)^{\mathbf{t}} \in \Omega$, where $p_0 \in \mathrm{R}$ is such that $\int_\Omega p = 0$ and we use again the same nonlinearity μ from Example 1 (cf. (4.1)). In this example, whereas that $\mathbf{u}$ is smooth, the variable p is singular along the line $x_1 = -0.1$, therefore, we should expect regions of high gradients along the line $x_1 = 0$. For this test, we make use of hexagonal meshes (see Figure 4.5).

First, we show that the adaptive methods decrease faster than those obtained by uniforms. This fact is better illustrated in Figure 4.2. In addition, the order of convergence of the estimator is shown in Figure 4.3. Also, the effectivity index remain bounded from above and below, which confirms the reliability and efficiency of $\boldsymbol{\eta}$. More precisely, we can observe that the effectivity for $\boldsymbol{\eta}$ is very near to 1, which is highly desirable because this determine the good quality of the estimator. Next, the Figure 4.4 show the orders of convergence of all variables under the refinement. We notice there that the rate of convergence $O(h^{k+1})$ is attained by all the unknowns, including the postprocessed $\mathbf{u}$ and p.

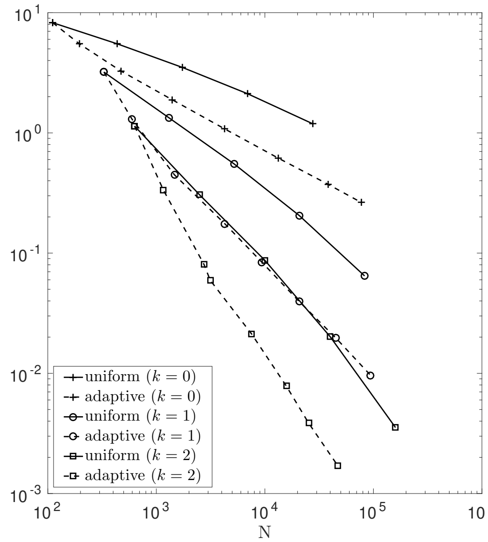

Figure 4.2: Example 2. Convergence history under uniform and adaptive refinement of the error $\mathsf{e}(\mathbf{u}, \mathbf{t}, \boldsymbol{\sigma})$ using hexagonal meshes.

Also, some intermediate meshes obtained with this adaptive strategy are displayed in Figure 4.5. Notice there that the adapted meshes concentrate the refinements along the line $x_1 = 0$, which means that the method is able to recognize the regions with high gradients of the solutions.

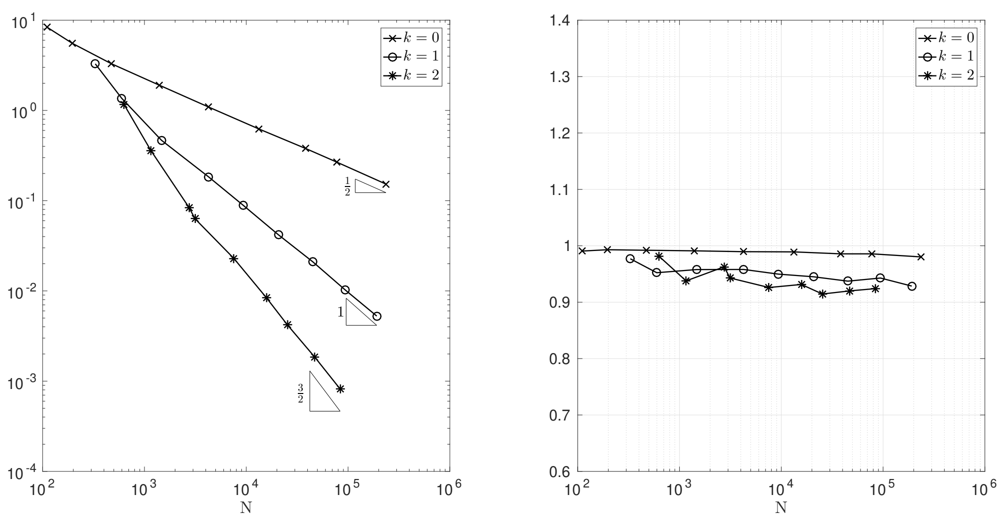

Figure 4.3: Example 2. Behavior under adaptive refinement (left). Effectivity of the estimator (right).

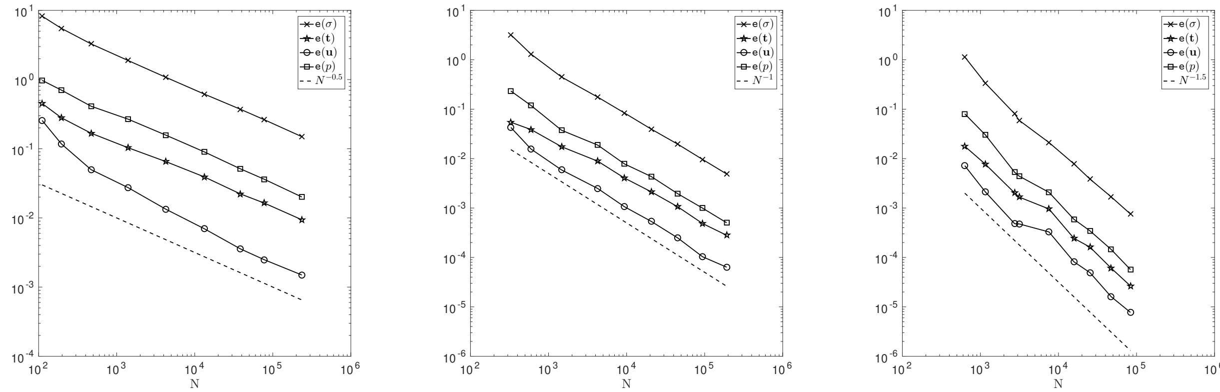

Figure 4.4: Example 2. Convergence history of the variables using an adaptive strategy based in the estimator $\boldsymbol{\eta}$.

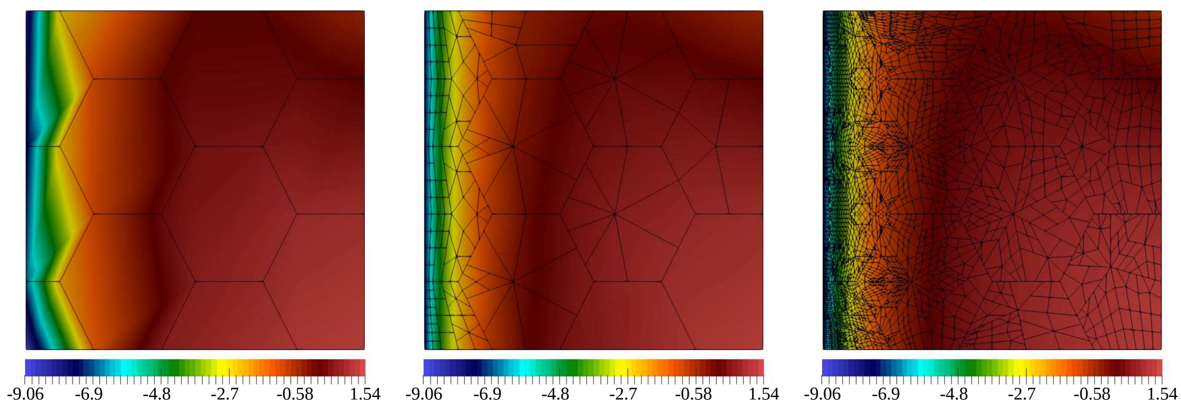

Figure 4.5: Example 2. Approximate pseudostress component $\boldsymbol{\sigma}^{\star}_{11,h}$. Some meshes from the adaptive refinement sequence obtained with $k = 1$: initial (left), after 3 refinement steps (center), and after 7 refinement steps (right).

4.3 Example 3

We take the L-shaped domain $\Omega := (-1,1)^2 \setminus (0,1)^2$, and choose $\mathbf{f}$ and $\mathbf{g}$ such that the exact solution is given by

$$\mathbf{u}(\mathbf{x}) \;:=\; \mathbf{curl}\Big(\sqrt{(x_1-0.01)^2+(x_2-0.01)^2}\Big) \qquad \text{and} \qquad p(\mathbf{x}) \;:=\; \frac{1}{x_2+1.1} - p_0$$

for all $\mathbf{x} := (x_1, x_2)^{\mathbf{t}} \in \Omega$, where $p_0 \in \mathrm{R}$ is such that $\int_\Omega p = 0$. Moreover, we consider the nonlinear viscosity μ given by

$$\mu(s) \;:=\; \frac{1}{2} + \frac{1}{2}(1+s^2)^{-1/4} \qquad \forall\, s \geq 0\,. \tag{4.2}$$

Note in this example that $\mathbf{u}$ and p are singular near to the origin, and along the line $x_2 = -1.1$, respectively. Hence, we should expect regions of high gradients around $(0,0)$, and along the line $x_2 = -1$. For this test, we use meshes composed of distorted squares (see Figure 4.9).

Firstly, as expected, the error of the adaptive method decrease faster than the obtained by the uniform one. This fact is illustrated in Figure 4.6. In addition, from Figure 4.7, we can observe

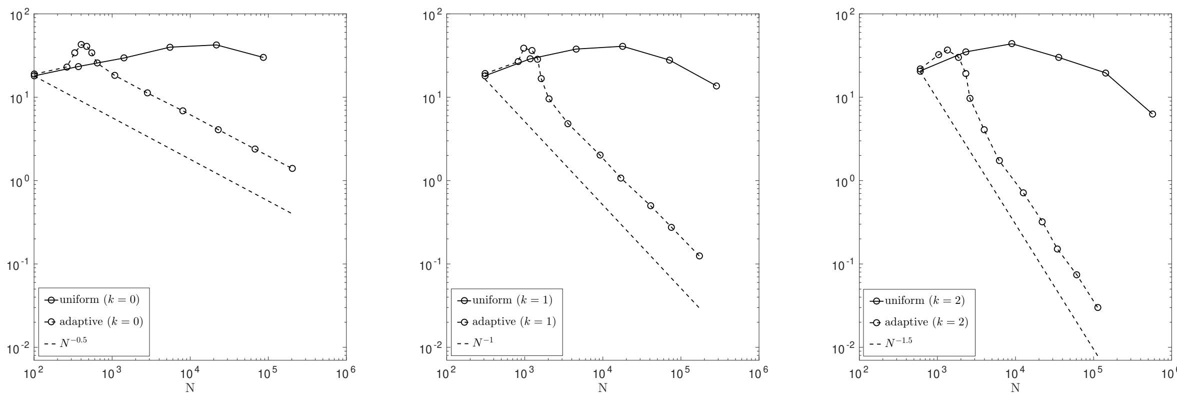

Figure 4.6: Example 3. Convergence history under uniform and adaptive refinement of the error $\mathsf{e}(\mathbf{u}, \mathbf{t}, \boldsymbol{\sigma})$ using the estimator $\boldsymbol{\eta}$ and meshes composed of distorted squares.

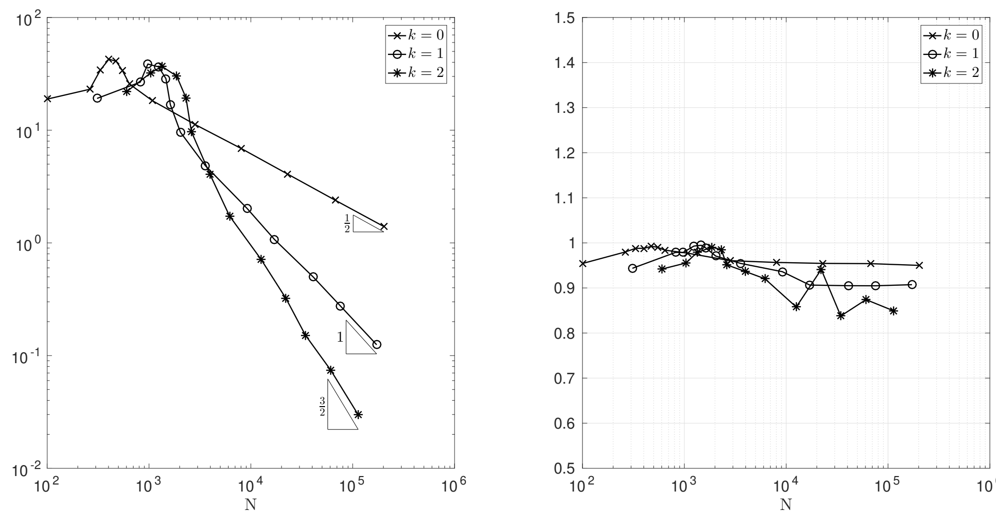

Figure 4.7: Example 3. Behavior under adaptive refinement (left). Effectivity of the estimator (right).

how the effectivity index remain again bounded from above and below, which confirms again the reliability and efficiency of the estimator for the associated adaptive algorithm as well. Here we can see a similar behavior to the observed in the Example 2, in connection with the optimality properties of the estimator. Also, the robustness with respect to the nonlinearity is established.

On the other hand, Figure 4.8 shows the orders of convergence of all variables under the refinement. We notice that the rate of convergence $O(h^{k+1})$ is attained by all the unknowns, including the postprocessed $\mathbf{u}$ and p. Finally, some intermediate meshes obtained with this adaptive strategy are displayed in Figures 4.9. Notice there that the adapted meshes concentrate the refinements around the origin and the line $x_2 = -1$, which means that the method is able to recognize the regions with high gradients of the solutions.

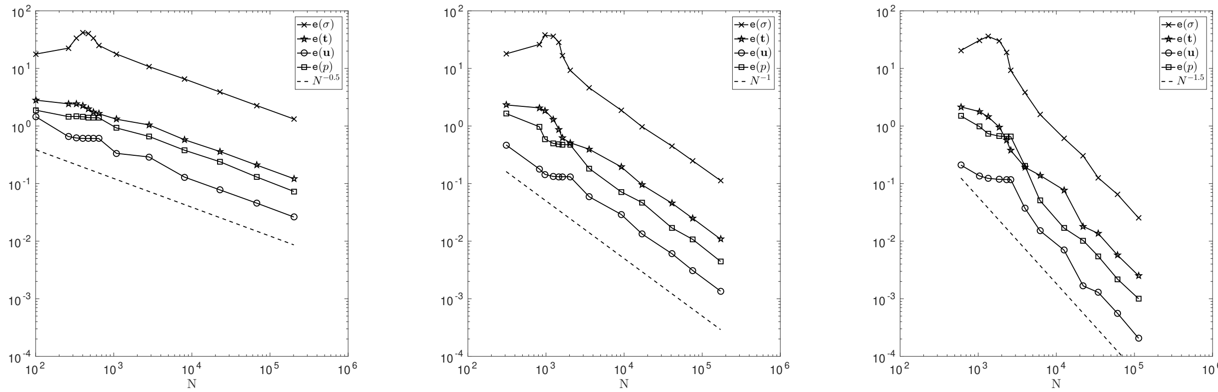

Figure 4.8: Example 3. Convergence history of the variables using an adaptive strategy based in the estimator $\boldsymbol{\eta}$.

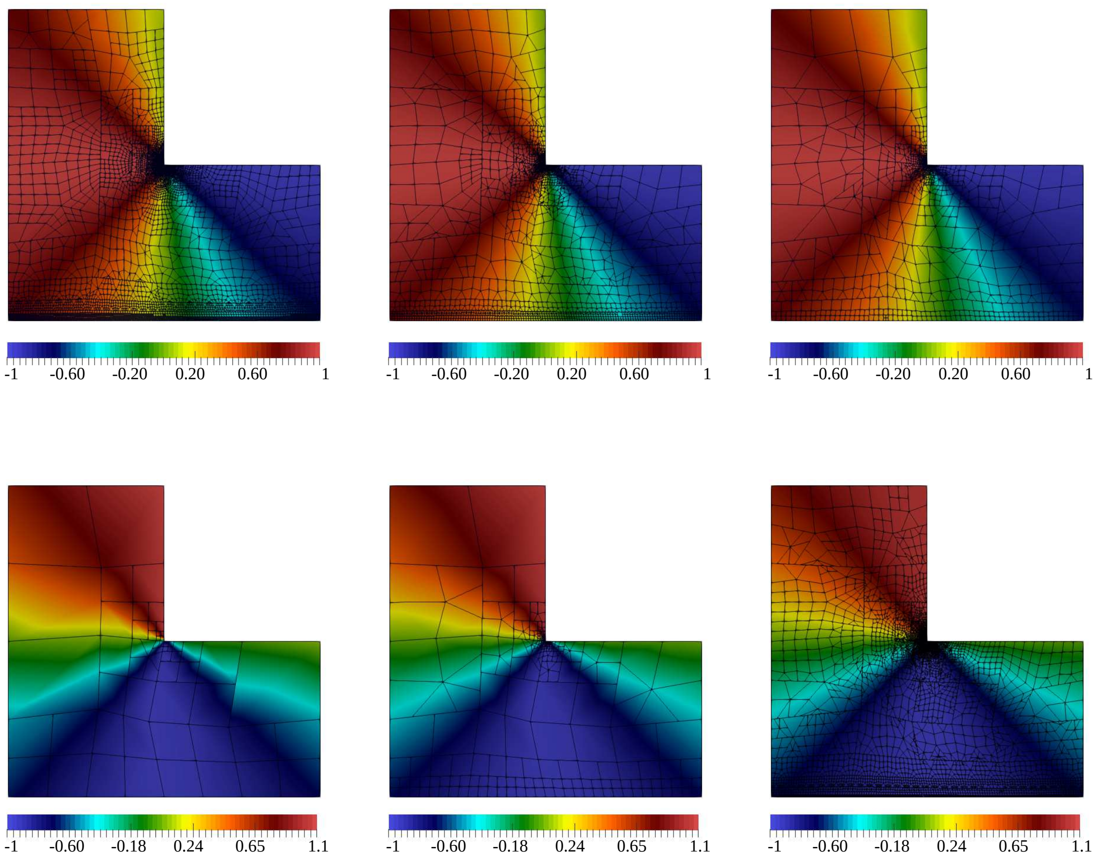

Figure 4.9: Example 3. Approximate velocity component $\mathbf{u}_{2,h}$. (Top) The mesh after eleven adaptive refinements with $k = 0$ (left), $k = 1$ (center) and $k = 2$ (right). Approximate velocity component $\mathbf{u}_{1,h}$ (Below) Some meshes from the adaptive refinement sequence obtained with $k = 1$: after 4 refinement steps (left), after 8 refinement steps (center), and after 12 refinement steps (right).

Acknowledgements

The authors would like to thank Gabriel N. Gatica, CI^{2}MA and Departamento de Ingeniería Matemática, Universidad de Concepción, Chile, for facilitating their collaboration. The work of Mauricio

Munar was partially supported by CONICYT-Chile through the project AFB170001 of the PIA Program: Concurso Apoyo a Centros Científicos y Tecnológicos de Excelencia con Financiamiento Basal, and the Becas-CONICYT Programme for foreign students, and by Centro de Investigación en Ingeniería Matemática (CI^{2}MA), Universidad de Concepción. The work of Filánder A. Sequeira was partially supported by Universidad Nacional, Costa Rica, through the project 0103-18.

References

[1] M. Alvarez, and G. N. Gatica and R. Ruiz-Baier, *A posteriori error analysis for a viscous flow-transport problem*. ESAIM Math. Model. Numer. Anal. 50 (2016), no. 6, 1789–1816.

[2] P. F. Antonietti, L. Beirão da Veiga, D. Mora, and M. Verani, *A stream virtual element formulation of the Stokes problem on polygonal meshes*. SIAM J. Numer. Anal. 52 (2014), no. 1, 386–404.

[3] L. Beirão da Veiga, F. Brezzi, A. Cangiani, G. Manzini, L. Marini, and A. Russo, *Basic principles of virtual element methods*. Math. Models Methods Appl. Sci. 23 (2013), no. 1, 199–214.

[4] L. Beirão da Veiga, F. Brezzi, L. Marini, and A. Russo, $H(\mathrm{div})$ *and* $H(\mathbf{curl})$*-conforming virtual element method*. Numer. Math. 133 (2016), no. 2, 303–332.

[5] ——, *Mixed virtual element methods for general second order elliptic problems on polygonal meshes*. ESAIM Math. Model. Numer. Anal. 50 (2016), no. 3, 727–747.

[6] L. Beirão da Veiga, C. Lovadina, and G. Vacca, *Divergence free virtual elements for the Stokes problem on polygonal meshes*. ESAIM Math. Model. Numer. Anal. 51 (2017), no. 2, 509–535.

[7] L. Beirão da Veiga, C. Lovadina, and G. Vacca, *Virtual elements for the Navier-Stokes problem on polygonal meshes*. SIAM J. Numer. Anal. 56 (2018), no. 3, 1210–1242.

[8] L. Beirão da Veiga and G. Manzini, *Residual a posteriori error estimation for the virtual element method for elliptic problems*. ESAIM Math. Model. Numer. Anal. 49 (2015), no. 2, 577–599.

[9] S. Berrone and A. Borio, *A residual a posteriori error estimate for the Virtual Element Method*. Math. Models Methods Appl. Sci. 27 (2017), no. 8, 1423–1458.

[10] F. Brezzi, R. S. Falk, and L. Marini, *Basic principles of mixed virtual element methods*. ESAIM Math. Model. Numer. Anal. 48 (2014), no. 4, 1227–1240.

[11] F. Brezzi and M. Fortin, *Mixed and Hybrid Finite Element Methods*. Springer Verlag, New York, 1991.

[12] E. Cáceres and G. N. Gatica, *A mixed virtual element method for the pseudostress-velocity formulation of the Stokes problem*. IMA J. Numer. Anal. 37 (2017), no. 1, 296–331.

[13] E. Cáceres, G. N. Gatica, and F. A. Sequeira, *A mixed virtual element method for the Brinkman problem*. Math. Models Methods Appl. Sci. 27 (2017), no. 4, 707–743.

[14] E. Cáceres, G. N. Gatica, and F. A. Sequeira, *A mixed virtual element method for quasi-Newtonian Stokes flows*. SIAM J. Numer. Anal. 56 (2018), no. 1, 317–343.

[15] A. Cangiani, E. H. Georgoulis, T. Pryer, and O. J. Sutton, *A posteriori error estimates for the virtual element method*. Numer. Math. 137 (2017), no. 4, 857–893.

[16] A. Cangiani, V. Gyrya, and G.Manzini, *The nonconforming virtual element method for the Stokes equations*. SIAM J. Numer. Anal. 54 (2016), no. 6, 3411–3435.

[17] A. Cangiani and M. Munar, *A posteriori error estimates for mixed virtual element methods*. Preprint 2019-10, Centro de Investigación en Ingeniería Matemática, Universidad de Concepción. [available at `http://www.ci2ma.udec.cl/publicaciones/prepublicaciones/`].

[18] H. Chi, L. Beirão da Veiga, and G. H. Paulino, *A simple and effective gradient recovery scheme and a posteriori error estimator for the virtual element method (VEM)*. Comput. Methods Appl. Mech. Engrg. 347 (2019), 21–58.

[19] G. N. Gatica, *A Simple Introduction to the Mixed Finite Element Method*. SpringerBriefs in Mathematics, Springer, Cham, 2014. Theory and applications.

[20] G. N. Gatica, L. F. Gatica, and F. A. Sequeira, *Analysis of an augmented pseudostress-based mixed formulation for a nonlinear Brinkman model of porous media flow*. Comput. Methods Appl. Mech. Engrg. 289 (2015), 104–130.

[21] G. N. Gatica, A. Márquez, and M. A. Sánchez, *Analysis of a velocity-pressure-pseudostress formulation for the stationary Stokes equations*. Comput. Methods Appl. Mech. Engrg. 199 (2010), no. 17-20, 1064–1079.

[22] ——, *A priori and a posteriori error analyses of a velocity-pseudostress formulation for a class of quasi-Newtonian Stokes flows*. Comput. Methods Appl. Mech. Engrg. 200 (2011), no. 17-20, 1619–1636.

[23] G. N. Gatica, M. Munar, and F. A. Sequeira, *A mixed virtual element method for a nonlinear Brinkman model of porous media flow*. Calcolo. 55 (2018), no. 2, Art. 21, 36 pp.

[24] G. N. Gatica, M. Munar, and F. A. Sequeira, *A mixed virtual element method for the Navier-Stokes equations*. Math. Models Methods Appl. Sci. 28 (2018), no. 14, 2719–2762.

[25] G. N. Gatica, M. Munar, and F. A. Sequeira, *A mixed virtual element method for the Boussinesq problem on polygonal meshes*. Preprint 2019-32, Centro de Investigación en Ingeniería Matemática, Universidad de Concepción. [available at `http://www.ci2ma.udec.cl/publicaciones/prepublicaciones/`].

[26] D. Irisarri and G. Hauke, *Stabilized virtual element methods for the unsteady incompressible Navier-Stokes equations*. Calcolo 56 (2019), no. 4, Art. 38, 21 pp.

[27] X. Liu and Z. Chen, *The nonconforming virtual element method for the Navier-Stokes equations*. Adv. Comput. Math. 45 (2019), no. 1, 51–74.

[28] X. Liu, J. Li and Z. Chen, *A nonconforming virtual element method for the Stokes problem on general meshes*. Comput. Methods Appl. Mech. Engrg. 320 (2017), 694–711.

[29] D. Mora, Rivera, and R. Rodríguez, *A posteriori error estimates for a Virtual Element Method for the Steklov eigenvalue problem*. Comput. Math. Appl. 74 (2017), no. 9, 2172–2190.

[30] D. Mora and G. Rivera, *A priori and a posteriori error estimates for a virtual element spectral analysis for the elasticity equations*. IMA Journal of Numerical Analysis. DOI: https://doi.org/10.1093/imanum/dry063.

[31] R. Oyarzúa, M. Solano, and P. Zúñiga, *A priori and a posteriori error analyses of a high order unfitted mixed-fem for Stokes flow.* Preprint 2019-15, Centro de Investigación en Ingeniería Matemática, Universidad de Concepción. [available at http://www.ci2ma.udec.cl/publicaciones/prepublicaciones/].

[32] G. Vacca, *An H^1-conforming virtual element for Darcy and Brinkman equations.* Math. Models Methods Appl. Sci. 28 (2018), no. 1, 159–194.

Centro de Investigación en Ingeniería Matemática (CI²MA)

PRE-PUBLICACIONES 2019

2019-34 Gabriel N. Gatica, Ricardo Oyarzúa, Nathalie Valenzuela: *A five-field augmented fully-mixed finite element method for the Navier-Stokes/Darcy coupled problem*

2019-35 Luis Miguel De Oliveira Vilaca, Bryan Gomez-Vargas, Sarvesh Kumar, Ricardo Ruiz-Baier, Nitesh Verma: *Advection-diffusion-reaction in poroelastic media. Part I: Well-posedness and discrete analysis*

2019-36 Carlo Lovadina, David Mora, Iván Velásquez: *A virtual element method for the von Kármán equations*

2019-37 Eligio Colmenares, Gabriel N. Gatica, Sebastian Moraga, Ricardo Ruiz-Baier: *A fully-mixed finite element method for the steady state Oberbeck-Boussinesq system*

2019-38 Eligio Colmenares, Gabriel N. Gatica, Willian Miranda: *Analysis of an augmented fully-mixed finite element method for a bioconvective flows model*

2019-39 Raimund Bürger, Paul E. Méndez, Ricardo Ruiz-Baier: *Convergence of H(div)-conforming schemes for a new model of sedimentation in circular clarifiers with a rotating rake*

2019-40 Peter Monk, Cinthya Rivas, Rodolfo Rodríguez, Manuel Solano: *An asymptotic model based on matching far and near field expansions for thin gratings problems*

2019-41 Sergio Caucao, Ricardo Oyarzúa, Segundo Villa-Fuentes: *A new mixed-FEM for steady-state natural convection models allowing conservation of momentum and thermal energy*

2019-42 Gonzalo A. Benavides, Sergio Caucao, Gabriel N. Gatica, Alejandro A. Hopper: *A new mixed-primal finite element method for a coupled flow-transport problem*

2019-43 Gabriel N. Gatica, Bryan Gomez-Vargas, Ricardo Ruiz-Baier: *A posteriori error analysis of mixed finite element methods for stress-assisted diffusion problems*

2019-44 Nestor Sánchez, Tonatiuh Sanchez-Vizuet, Manuel Solano: *A priori and a posteriori error analysis of an unfitted HDG method for semi-linear elliptic problems*

2019-45 Mauricio Munar, Filander A. Sequeira: *A posteriori error analysis of a mixed virtual element method for a nonlinear Brinkman model of porous media flow*

Para obtener copias de las Pre-Publicaciones, escribir o llamar a: Director, Centro de Investigación en Ingeniería Matemática, Universidad de Concepción, Casilla 160-C, Concepción, Chile, Tel.: 41-2661324, o bien, visitar la página web del centro: http://www.ci2ma.udec.cl




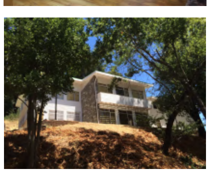

Centro de Investigación en Ingeniería Matemática (CI^{2}MA)

Universidad de Concepción

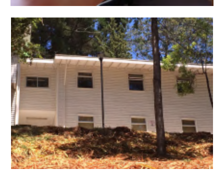

Casilla 160-C, Concepción, Chile
Tel.: 56-41-2661324/2661554/2661316
http://www.ci2ma.udec.cl